Integrated Sensing from Multiple Wearable Devices for Activity Recognition and Dead Reckoning

by

Darrell Loh

B.A.Sc., Simon Fraser University, 2011

Thesis Submitted in Partial Fulfillment of the
Requirements for the Degree of
Master of Applied Science

in the
School of Mechatronic Systems Engineering
Faculty of Applied Sciences

SIMON FRASER UNIVERSITY

Spring 2016

Approval

Name:	**Darrell Loh**
Degree:	**Master of Applied Science**
Title:	***Integrated Sensing from Multiple Wearable Devices for Activity Recognition and Dead Reckoning***
Examining Committee:	**Chair: Behraad Bahreyni** Associate Professor

Edward J. Park
Senior Supervisor
Professor _____

Reynald Hoskinson
Supervisor
Research Associate _____

Flavio Firmani
Internal Examiner
Lecturer _____

Date Defended/Approved: March 9th, 2016

Ethics Statement

The author, whose name appears on the title page of this work, has obtained, for the research described in this work, either:

a. human research ethics approval from the Simon Fraser University Office of Research Ethics,

or

b. advance approval of the animal care protocol from the University Animal Care Committee of Simon Fraser University;

or has conducted the research

c. as a co-investigator, collaborator or research assistant in a research project approved in advance,

or

d. as a member of a course approved in advance for minimal risk human research, by the Office of Research Ethics.

A copy of the approval letter has been filed at the Theses Office of the University Library at the time of submission of this thesis or project.

The original application for approval and letter of approval are filed with the relevant offices. Inquiries may be directed to those authorities.

Simon Fraser University Library
Burnaby, British Columbia, Canada

update Spring 2010

Abstract

Wearable devices are increasingly prevalent in our everyday lives. This thesis examines the potential of combining multiple wearable devices worn on different body locations for fitness activity recognition and inertial dead-reckoning. First, a novel method is presented to classify fitness activities using head-worn sensors, with comparisons to other common worn locations on the body. Using multiclass Support Vector Machine (SVM) on head-worn sensors, high degree of accuracy was obtained for classifying standing, walking, running, ascending/descending stairs and cycling. Next, a complete inertial dead-reckoning system for walking and running using smartwatch and smartglasses is proposed. Head-turn motion can derail the position propagation on a head-worn dead-reckoning system. Using the relative angle rate-of-change between arm swing direction and head yaw, head-turn motion can be detected. The experimental results show that using the proposed head-turn detection algorithm, head-worn dead-reckoning performance can be greatly improved.

Keywords: inertial sensors; wearable devices; sensor fusion; human activity recognition (HAR); pedestrian dead reckoning (PDR);

To my parents - my biggest supporters since day one.

Acknowledgements

Pursuing my master's degree has been my biggest and most meaningful challenge so far. It would not be possible without my supervisor – Dr Edward Park. I am eternally grateful to Dr Park for these two and a half years. His guidance in helping me improve as a researcher - from teaching me proper research methodology, planning experimental data collection to editing my scientific papers to make it 10 times better! These skills will be invaluable in life even long after academia.

I would also like to thank my close research collaborators – Shaghayegh and Matthew. Bouncing ideas off them made me more confident in my research ideas. My research group who made life in the lab more enjoyable – Paul, Magnus and Ahmed.

Special thanks to Reynald and Hamid, my industrial supervisors, who taught me thinking about the practicality aspect of research.

Last but not least, to all the test participants who willingly exert themselves for my data collection, all without monetary rewards – THANK YOU!

Table of Contents

List of Tables

List of Figures

List of Acronyms

ADL	Activities of Daily Living
BLE	Bluetooth low energy
ENU	East, North and Up
FN	False Negative
FP	False Positive
GNSS	Global Navigation Satellite System
GPS	Global Positioning System
HAR	Human Activities Recognition
MEMS	Microelectromechanical Systems
OHMD	Optical Head-mounted Device
PCA	Principal Component Analysis
PDR	Pedestrian dead reckoning
SVM	Support Vector Machines
TN	True Negative
TP	True Positive

Chapter 1.

Introduction

1.1. Background and Motivation

Wearable technology has taken the consumer market by storm in recent years. The industry is projected to grow substantially within the next decade [1]. Traditionally, wearable sensors are worn on the wrists, waist/hip or strapped onto shoelaces. Wrist-worn devices such as Android Wear-based watches (Figure 1.1), Apple Watch, Fitbit, Microsoft Band and Garmin GPS watches are among the most popular wearable devices. Recently, the emergence of smartglassess like Recon Jet (Figure 1.1) and Google Glass provides an extra dimension in non-intrusive body locations. In a survey of 6000 consumers across six countries, more than 40% of the respondents are interested in wearable eyeglasses [2]. In fact, according to an online database that tracks wearable devices available on the market [3], out of the 434 wearable devices listed, 204 (47.0%) are wrist-worn devices, followed by 79 (18.2%) head-worn devices and 25 (5.8%) devices worn on the torso. With the breadth of wearable devices' market penetration, this calls for an investigation into fusing multiple wearable devices for two meaningful

Figure 1.1. LG G Watch R (left) and Recon Jet (right)

research areas – Human activity recognition (HAR) and Pedestrian dead reckoning (PDR).

Human activity recognition is an increasingly popular research area, fuelled by the development of low-cost, miniature sensors within the last decade [4]. HAR is an attractive area of research because it can benefit a wide variety of industries, such as health care, fitness and even the entertainment sector. In the health care industry, caregivers can monitor and assess patients' progress more continuously and effectively with information from activities of daily living (ADL) [5]. In fitness applications, fitness software can estimate the user's calorie expenditures more precisely given the context of user's activities.

Global Navigation Satellite System (GNSS) positioning is the most common outdoor positioning. However, GNSS solution degrades in areas with tall buildings due to signal blockage and multipath error. This is where inertial dead reckoning can improve performance of absolute positioning by propagating the position from a previously known position. Pedestrian dead reckoning is a widely studied subject, due to the immensely beneficial applications that span from tracking people with special needs such as elderly, children, and the vision impaired, to public safety services such as policemen and firefighters [6], [7]. It is also invariantly driven by the availability of small, low-cost microelectromechanical systems (MEMS) inertial sensors [7] that have seen their accuracy and cost improve significantly in the previous decade [8].

In this thesis, the potential of combining multiple wearable devices worn on different body locations is examines for improved fitness activity recognition and inertial dead-reckoning.

1.2. Literature Review

While there are many HAR research using inertial sensors, most of them focus on sensor placements on the trunk or the limbs. Bao and Intille [9] tested sensor

placements on the arm, wrist, hip, thigh and ankle with overall accuracies of over 84% in classifying 20 activities by using all five sensor locations. Ishimaru et al. [10] suggested that head-worn sensors have not been prominent in the past HAR research, possibly because of the obtrusiveness of previously available devices. They took the opportunity of using Google's less obtrusive Glass smart glasses to test the feasibility of using head motion and eye blink frequency for activity recognition. However, only low-level activities (e.g., reading and talking) and no fitness activities were included in that study. Another head-mounted HAR study was done by Lo et al., who used ear-worn sensor (e-AR) for their studies and showed an average accuracy of 87% for reading, walking, lying and running [11], [12]. Activities that include vertical motions, such as walking on an incline or climbing stairs are typically hard to detect using just inertial sensors. Anastasopoulou et al. showed excellent results when a barometric pressure sensor is combined with inertial sensors mounted on the waist [13], with average accuracy of 98.2% in classifying 7 activities.

Pedestrian inertial dead reckoning can usually be categorized as self-contained and aided navigation [14]. The self-contained navigation, which is based on only inertial sensors, tends to drift over time. This drift is due to the integration of uncompensated time-varying bias of the low-cost, consumer grade MEMS inertial sensors. Thus, self-contained navigation must be aided by an absolute positioning system for practical long-term usage. For aided inertial navigation, GNSS [15] and cellular networks are typically used for outdoor navigation, while Wi-Fi [16], [17], Bluetooth, ultra-wideband (UWB) [18], [19], or even ultrasonic ranging [20] are used for indoor navigation. When the building map information is available, it can also be used for map-matching purposes [7], [21].

Previous inertial dead reckoning approaches in the literature are mainly based on sensors located on the foot [15], [20], [22]. This is because a foot-mounted IMU can provide frequent ground contact information, which helps to reduce drift. Some researchers have used waist-mounted sensors for dead reckoning [23]–[25] due to its closeness to the center-of-mass and because it can provide human stance or posture information. On the other hand, a wrist or head-worn device in the form of glasses or a watch is more user-friendly and acceptable compared to a foot or waist-worn device. However, head and wrist-worn devices have not been well-investigated for inertial dead

reckoning due to the complication of the head/wrist movements irrespective of the subject's moving direction. Some research has explored the use of helmet-mounted sensors for pedestrian dead reckoning, but with the assumption that the head and body is a rigid system (i.e. the head facing in the direction of motion) [6]. Other head-worn navigation related studies include using laser scanner for Simultaneous Localization and Mapping (SLAM) [26], [27].

1.3. Research Objectives and Contributions

The research objectives of this thesis are comprised of two distinct research areas – human activities recognition (HAR) and pedestrian dead reckoning (PDR). The common theme in this thesis is fusing the low-cost MEMS sensors found on multiple wearable device combinations. The scope of this thesis is geared towards fitness applications, with the proposed HAR classifying standing, walking, running, cycling, ascending/descending stairs while the proposed PDR is specific to walking and running.

In contrast to previous HAR works which concentrate mostly on trunk-based sensors, this thesis presents a novel method to classify six physical activities by using head-worn accelerometer, gyroscope, barometric pressure sensor and GPS. Furthermore, classification performance of various sensor location combinations is also presented for comparison purposes.

For a PDR that is more dedicated to fitness applications such as walking and running, one can exploit the cyclic nature of the natural arm swing motion during these activities (Figure 1.2). Arm swing during human locomotion is a natural motion that is linked to lower body dynamics. It is suggested that arm swing during locomotion contribute to the overall gait stability of human locomotion [28], [29]. The main contribution of this thesis is to present a novel algorithm that exploits the cyclic nature of arm swing during walking and running, combined with head-worn sensors to improve the accuracy of an inertial dead reckoning system.

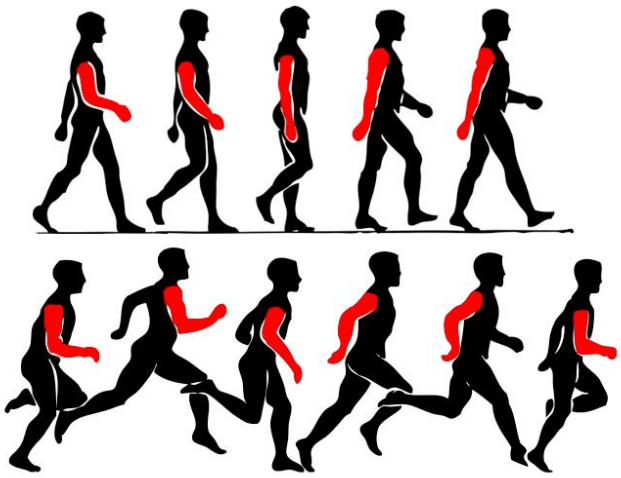

Figure 1.2. Arm swing in human locomotion during walking (top) and running (bottom)

1.4. Thesis Outline

This thesis is consists of the following four chapters.

In **Chapter 1**, the HAR and PDR research topics are introduced along with the current state-of-the-art in research. This thesis' research objective and contributions are also outlined.

In **Chapter 2**, a HAR algorithm using head-worn sensors is proposed. The proposed HAR method is tested on 8 test subjects, and compared with HAR using different combination of sensor body locations.

In **Chapter 3**, a complete PDR technique including step counting, step length estimation, head rotation detection and dead reckoning using the combination of smartwatch and smartglasses is presented.

In **Chapter 4**, this thesis is concluded with a summary of each chapter, followed by suggestions for future works.

Chapter 2.

Fitness Activity Classification by Using Multiclass Support Vector Machines on Head-worn Sensors

2.1. Introduction

Fitness activity classification on wearable devices can provide activity-specific information and generate more accurate performance metrics. Recently, optical head-mounted displays (OHMD) like Google Glass, Sony SmartEyeglass and Recon Jet have emerged. This chapter presents a novel method to classify fitness activities using head-worn accelerometer, barometric pressure sensor and GPS, with comparisons to other common mounting locations on the body.

This chapter is organized as follows. Sec. 2.2 details the experimental procedures, the measurement systems and the test subjects' statistics. Sec. 2.3 describes the proposed Multiclass Support Vector Machines (SVM) and the features being used. Sec. 2.4 shows the results and discussions of the results. Finally, Sec. 2.5 concludes this chapter with ideas for future works.

2.2. Data Collection

2.2.1. Experimental procedure

The data collection took place indoors at Simon Fraser University's Surrey campus and outdoors at a nearby park. Each participant was directed to complete the activities listed in Table 2.1. The participants walked and ran at their own paces. In the cycling segment, the participants were encouraged to perform normal cycling maneuvers like cycling while seated, riding out of the saddle and the occasional coasting. During the whole experiment, the participants were encouraged to act as naturally as possible, and they were allowed to rotate their head or gesture with their hands as they normally would.

Table 2.1. Data Collection Protocol

Environment	Activity	Approx. duration (min)
Indoor	Standing	3
	Walking	10
	Ascending stairs	2
	Descending stairs	2
Outdoor	Standing	3
	Walking	10
	Running	5
	Cycling	10
	Total time	**45**

2.2.2. Measurement Systems

Five inertial measurement units (IMUs), 4 MTx and 1 MTi-G from Xsens Technologies were used in the experiments (Figure 2.1). Both IMUs provide tri-axial acceleration and angular velocity measurements, with the MTi-G providing the additional GPS speed and horizontal dilution of precision (HDOP). The inertial data was collected at 100Hz, while the GPS data was collected at 4Hz. The MTi-G was mounted onto a

helmet, while the four MTx were strapped to the subject's left arm, left wrist, left pant pocket and left ankle. The IMUs were connected to a laptop inside a backpack. A GoPro Hero3 camera was attached onto the helmet for tagging the activities.

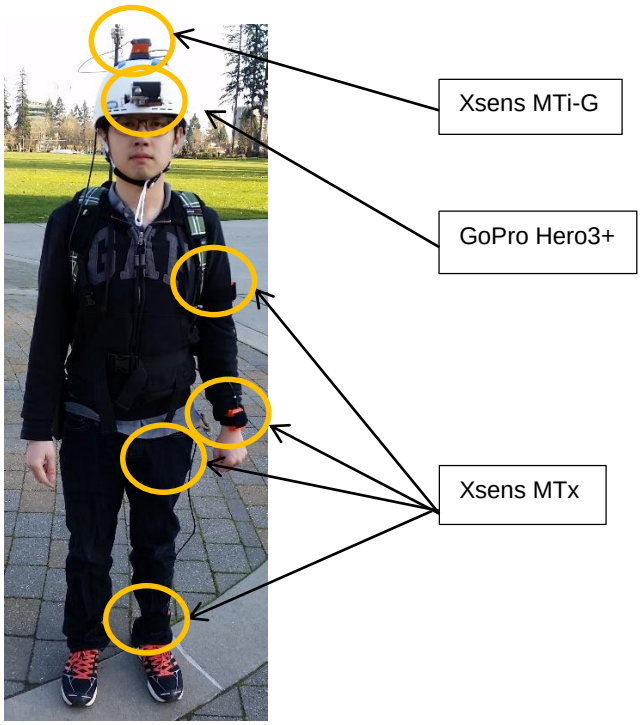

Figure 2.1. Sensors placement on head, arm, wrist, trouser pocket and ankle

2.2.3. Test Subjects

Eight healthy participants were recruited for the data collection experiments. The only requirements were that they can comfortably run and bike continuously for at least 10 minutes. The participant group consisted of 5 males and 3 females, with an average age of 25.63±6.18 years old, an average height of 168.61±10.16 cm and an average weight of 61.77±15.99 kg. All the participants agreed and signed the participant consent form approved by Simon Fraser University's Research Ethics Board.

2.3. Data Analysis

All sensor data collected was tagged according to the participant's activities using the GoPro video footage. Transitional motions like opening a door and mounting a bicycle were excluded from this study.

2.3.1. Data Preprocessing

The sensor signals were segmented into 2-second windows with 50% overlap. The 2-second window period is chosen because some stairs have steps between landings that often last less than a few seconds (Figure 2.2). The sensor data from Xsens IMUs are pre-calibrated and filtered, so no additional filtering was required.

Figure 2.2. A short flight of stairs between floor and stair landing

2.3.2. Feature Extraction

For every 2-second window, 12 key features were extracted from the following sensors:

Accelerometer

Common time domain features like mean, standard deviation (STD), mean absolute deviation (MAD) and percentile (10^{th}, 25^{th}, 50^{th}, 70^{th} and 90^{th}) [4] were computed from the magnitude of the 3-axis acceleration measurements. Frequency

domain feature like energy calculated from Fast Fourier Transform was also included as it has been shown to be effective for activity recognition [9].

The features described can be computed using the equations below [4]:

$$\text{Mean: } \overline{y} = \frac{1}{n} \tag{2.1}$$

$$\text{STD: } \sigma = \sqrt{\frac{1}{n-1}\sum_{i=1}^{n}(y_i - \overline{y})^2} \tag{2.2}$$

$$\text{MAD: } \sqrt{\frac{1}{n-1}\sum_{i=1}^{n}|y_i - \overline{y}|} \tag{2.3}$$

$$k\text{th Percentile: } P_k = \frac{nk}{100} + 0.5 \tag{2.4}$$

$$\text{Energy: } \frac{\sum_{i=1}^{n} F_i^2}{n} \tag{2.5}$$

Barometer

The slope of the barometric pressure measurements in the 2-second window was calculated using least squares linear regressions. The slope, a_1 in a linear equation $y(t) = a_0 + a_1(t)$ can be found by first fitting the barometric data using least square [30]

$$A = (X^T X)^{-1} X^T Y \tag{2.6}$$

where $= \begin{bmatrix} a_0 \\ a_1 \end{bmatrix}$, $X = \begin{bmatrix} 1 & t_1 \\ 1 & t_2 \\ \vdots & \vdots \\ 1 & t_n \end{bmatrix}$ and $Y = \begin{bmatrix} y_1 \\ y_2 \\ \vdots \\ y_n \end{bmatrix}$

The standard deviation of the barometric pressure measurements was also used.

GPS

A 2-second average of horizontal GPS speed is used. To accommodate indoor environments with poor or no satellite visibility, the average GPS speed is extracted based on horizontal dilution of precision (HDOP), as shown in Figure 2.3.

```
1:   for all HDOP hdop_i in window
2:       if hdop_i < 5
3:           gpsSpeedSum += gpsSpeed_i
4:           n++;
5:       endif
6:   endfor
7:   if n==0
8:       windowGpsSpeed = -1;
9:   elseif
10:      windowGpsSpeed = gpsSpeedSum/n
11:  endif
```

Figure 2.3. Pseudocode for extracting GPS speed in 2-second signal window.

Sensor Fusion

In addition to the individual sensors, sensor-fused vertical speed is computed using a Kalman filter (KF) algorithm from our previous work [31] (See Appendix B). This KF algorithm uses accelerometer, gyroscope and barometric pressure sensor measurements to estimate the vertical speed. In a sample vertical speed plot from the experiment (Figure 2.4), larger negative peaks can be observed when a test subject is walking down the stairs (shaded areas *a* and *c*) versus walking on flat surface (non-shaded areas *b* and *d*). Furthermore, the shaded-area *c* shows four negative peaks, which corresponds to the four stair steps shown in the screenshot of Figure 2.2.

From vertical speed estimations, 4 additional features are extracted: the mean, standard deviation, maximum and minimum for each 2-second interval. Since the pressure sensor is only available on the Xsens MTi-G, the vertical speed was computed only for the head-worn sensor.

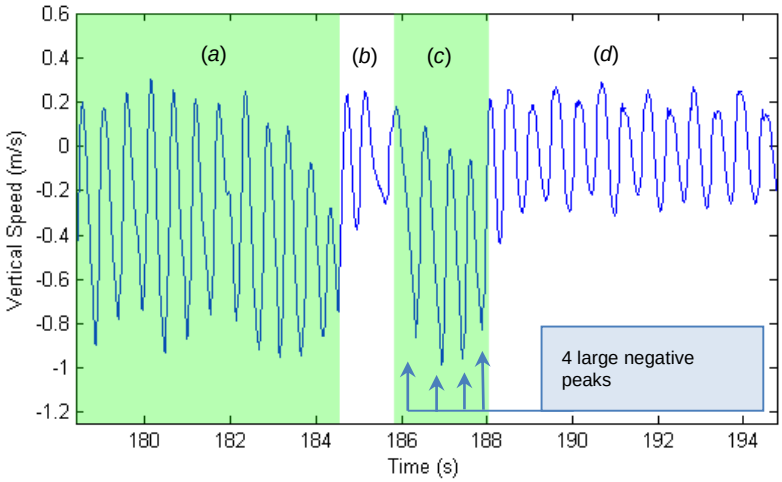

Figure 2.4. Estimated vertical speed using head-worn sensors when descending stairs (shaded) and flat surface (non-shaded)

Summary

The summary of all the features used are listed in Table 2.2

Table 2.2. Summary of Feature Extraction

Feature number	Description	Sensor(s)
1	Mean	Accelerometer
2	Standard deviation	
3	Mean absolute deviation	
4-8	Percentile	
9	FFT energy	
10	Slope	Barometer
11	Standard deviation	
12	GPS speed	GPS
13	Vertical speed mean	Accelerometer, gyroscope & barometer
14	Vertical speed standard deviation	
15	Vertical speed max	
16	Vertical speed min	

2.3.3. Classification: Support Vector Machines

A support vector machine (SVM) constructs a hyper-plane or set of hyper-planes in a high or infinite dimensional space, which can be used for classification or regression [32], [33]. SVM is versatile as it can be adapted to different classification problems using different Kernel functions (i.e. Linear, polynomial, radial basis function (RBF) and sigmoid).

The multiclass Support Vector Machines classifier implemented in LIBSVM [34] is used through the MATLAB interface. SVM is fundamentally a two-class classifier, but various methods have been developed to solve multiclass problems. LIBSVM uses the "one-against-one" approach [34], [33] for multiclass classifier. The RBF kernel is selected as it shows higher accuracy compared to other basis functions. To tune the parameters C and γ for the RBF, a coarse grid-search is used, with exponentially growing sequences of C and γ (i.e.: $C = 2^{-5}, 2^{-3}, .., 2^{15}$ and $\gamma = 2^{-15}, 2^{-13}, .., 2^{3}$). Finer grid searches were then used to search around the vicinity of the coarse grid-search results. The C and γ pair with the best 10-fold cross-validation was found to be C = 100 and $\gamma = 0.1$.

2.4. Evaluation

To evaluate our proposed fitness activity classification algorithm, the one-versus-all validation method is used. The one-versus-all verification can assess the generalizability of results across all subjects [11]. Classification results are commonly presented in a confusion matrix (Table 2.3).

Table 2.3. Confusion Matrix Example

		Predicted Class	
		Class A	Class B
Actual Class	Class A	True Positive (TP)	False Negative (FN)
	Class B	False Positive (FP)	True Negative (TN)

Recall, precision and f-measure are used as the performance metrics, as the class imbalance will skew the accuracy ratings [35]. They are calculated as follows:

$$\text{Recall: } \frac{TP}{TP+FN} \tag{2.7}$$

$$\text{Precision: } \frac{TP}{TP+FP} \tag{2.8}$$

$$\text{F-measure: } 2 \cdot \frac{precision \cdot recall}{precision+recall} \tag{2.9}$$

2.4.1. Results and discussions

Table 2.4 shows the confusion matrix for the head-worn sensor. The recall and precision for standing, walking, running and cycling are over 98%. Only ascending and descending stairs have lower precision and recall, as they are often confused with walking. This may be due to the noise in barometric pressure measurement and the similarity energy and gait frequency in walking and ascending/descending stairs. Ascending stairs performance is also significantly worse than descending stairs. This might be due to higher measurable impact when descending stairs. Larger vertical speed is also observed when descending stairs compared to ascending stairs.

The usage of sensor-fused vertical speed as a feature in the head-worn sensors showed a big improvement in classifying ascending and descending stairs (Table 2.5): The F-measure of ascending/descending stairs increased from 82.85%/87.50% to 87.19%/95.74%, bringing the average up from 94.43% to 96.66%. All in all, the head-worn sensors show excellent results to be used in fitness activity recognition.

Table 2.4. Confusion Matrix for Head-worn Sensors

		Classified as						
		Standing	***Walking***	***Running***	***Ascending Stairs***	***Descending Stairs***	***Cycling***	***Recall***
Actual activity	***Standing***	2620 s	1 s	1 s	1 s	0	4 s	99.73%
	Walking	0	9138 s	0	69 s	18 s	9 s	98.96%
	Running	2 s	0	2138 s	1 s	1 s	1 s	99.77%
	Ascending Stairs	0	46 s	0	446 s	9 s	3 s	88.49%
	Descending Stairs	0	12 s	0	0	461 s	0	97.46%
	Cycling	39 s	17 s	5 s	2 s	1 s	4583 s	98.62%
	Precision	98.46%	99.18%	99.72%	85.93%	94.08%	99.63%	

For further comparison purposes, the results of different sensors location combinations are evaluated. Table 2.5 shows the f-measure of all 31 sensor location combinations. For the case of one sensor, the ankle-strapped sensor performed the best, as can be expected from gait-based activities. Sensor worn on the head has the second highest f-measure, followed by the arm-strapped sensors. This coincides with the findings from Attala et al. [12], who suggested that the ear, arm and knee sensors are suitable for high-level activities such as running and cycling. The sensor inside the trouser pocket did not perform as well as the knee-strapped sensor. One factor might be because the sensor in the pocket was not strapped on, and some subjects wore loose fitting pants, resulting in the sensor moving relative to the leg.

In the case of two-sensor combinations, head + ankle, arm + ankle and wrist + ankle show average f-measure of more than 97%. Bao et al. [9] reached a similar conclusion that having only two accelerometers on upper and lower body is effective for human activity recognition. For the cases of three, four and five sensors combinations, there was no visible improvement over the best of the two-sensor combination.

Table 2.5. F-measure of All Sensors Location Combination

Sensor Combination	F-measure of Activity Classification						
	Standing	*Walking*	*Running*	*Asc. stairs*	*Des. stairs*	*Cycling*	*Average*
One sensor							
Head	99.05	98.43	99.67	82.85	87.50	99.07	94.43
Head (with vertical velocity)	99.09	99.07	99.74	87.19	95.74	99.12	96.66
Arm	98.64	97.40	99.46	56.75	91.15	99.30	90.45
Wrist	98.01	96.22	98.77	35.73	81.29	99.32	84.89
Pocket	98.51	95.30	98.35	43.12	75.13	99.01	84.90
Ankle	98.28	99.12	99.37	91.64	92.66	99.37	96.74
Two sensors							
Head + arm	99.13	98.44	99.49	78.56	91.79	99.23	94.44
Head + wrist	99.11	98.07	99.81	75.59	83.33	99.38	92.55
Head + pocket	98.94	97.70	99.74	78.99	83.32	98.70	92.90
Head + ankle	98.92	99.29	99.65	96.88	91.13	99.24	97.52
Arm + wrist	98.75	97.23	99.13	51.55	89.99	99.44	89.35
Arm + pocket	98.56	97.11	99.53	56.47	90.81	99.27	90.29
Arm + ankle	98.51	99.34	99.58	95.77	94.78	99.45	97.90
Wrist + pocket	98.56	95.08	99.07	41.95	69.45	99.41	83.92
Wrist + ankle	98.27	99.40	99.60	94.37	96.45	99.44	97.92
Pocket + ankle	98.34	98.94	99.32	88.31	95.18	99.34	96.57
Three sensors							
Head + arm + wrist	99.03	98.08	99.53	74.50	88.94	99.41	93.25
Head + arm + pocket	98.92	97.70	99.63	74.18	90.52	98.80	93.29
Head + arm + ankle	98.81	99.37	99.63	95.90	94.09	99.35	97.86
Head + wrist + pocket	98.86	97.27	99.67	76.25	75.17	99.17	91.07
Head + wrist + ankle	98.83	99.24	99.56	96.37	90.36	99.22	97.26
Head + pocket + ankle	98.88	98.88	99.53	94.58	86.12	99.19	96.20
Arm + wrist + pocket	98.49	97.14	99.44	58.31	89.12	99.46	90.33
Arm + wrist + ankle	98.45	99.30	99.65	96.68	93.40	99.46	97.82
Arm + pocket + ankle	98.41	98.71	99.51	88.66	91.68	99.43	96.07
Wrist + pocket + ankle	98.43	99.16	99.30	93.47	95.32	99.44	97.52
Four sensors							
Head + arm + wrist + pocket	98.73	97.86	99.60	76.97	86.36	99.31	93.14
Head + arm + wrist + ankle	98.64	99.33	99.67	96.18	92.96	99.47	97.71
Head + arm + pocket + ankle	98.60	98.92	99.65	93.60	89.18	99.40	96.56
Head + wrist + pocket + ankle	98.90	98.78	99.58	95.63	83.25	99.35	95.92
Arm + wrist + pocket + ankle	98.62	99.02	99.39	95.04	90.70	99.55	97.05
Five sensors							
Head + arm + wrist + pocket + ankle	98.66	98.97	99.65	95.18	87.88	99.53	96.64

2.5. Conclusion

In this chapter, a novel method is presented for classifying fitness activities using head-worn sensors. In comparison to other common sensors locations, the head-worn sensors shows good results that are suitable for fitness activity classification, provided that they are not too obtrusive for use (which is expected of the next generation smart eyeglasses). Two-sensor combinations of upper-body and ankle showed the best performance, with additional sensors not providing much improvement.

Chapter 3.

Inertial Dead Reckoning with Smartglasses and Smartwatch

3.1. Introduction

Wearable miniature inertial sensors have been widely used for inertial dead reckoning. Typical low-cost inertial dead reckoning systems use sensors attached to either the human trunk or feet. The recent emergence of smartglasses and smart watches provides an opportunity to use both types of wearable devices in position tracking. This chapter proposes a novel method of utilizing both a smartwatch and smartglasses for pedestrian dead reckoning. The general idea is to use the relative angle between arm swing direction and head yaw to detect any head-turn motion that would otherwise skew the position dead reckoning propagation. A complete inertial dead reckoning solution that includes step detection, step length estimation, head-rotation detection, and dead reckoning using a smartwatch and smartglasses that are currently available in the market is presented.

The overall flow of this chapter is as follows. In Sec. 3.2, the architecture of the proposed dead reckoning system is presented. The data collection method is described in Sec. 3.3, followed by the experimental results and discussions in Sec. 3.4. Finally, Sec. 3.5 concludes this chapter.

3.2. System Architecture

The overall block diagram of the proposed head-wrist pedestrian dead reckoning (HWPDR) system is shown in Figure 3.1. The following subsections describe each sub-block of the system in detail.

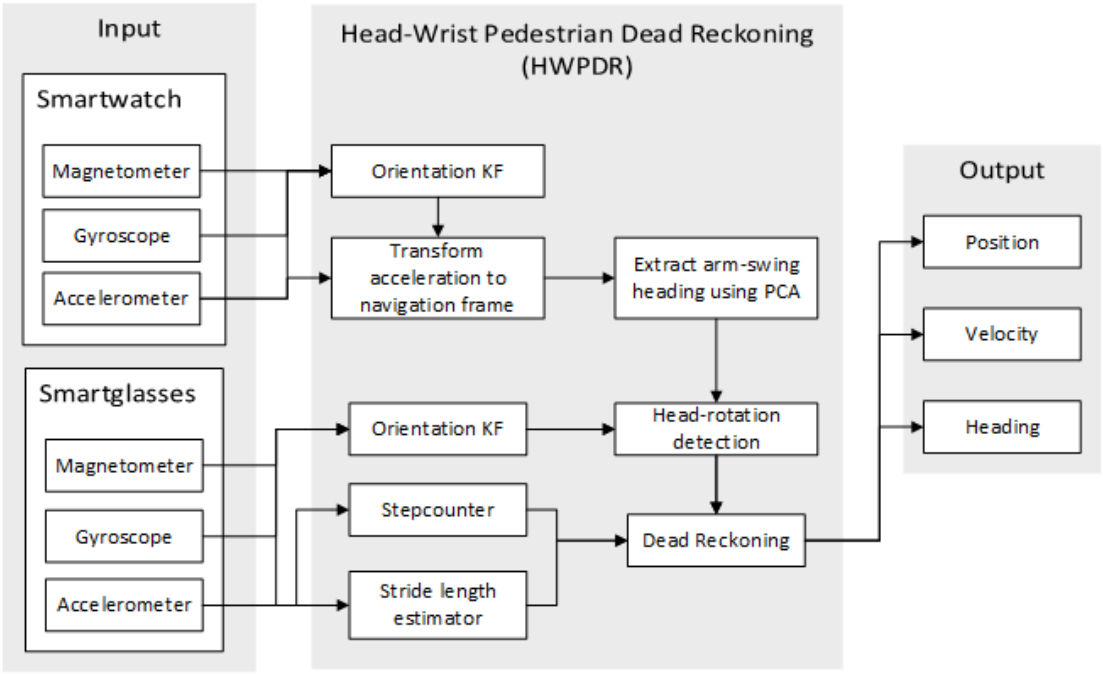

Figure 3.1. Proposed head-wrist pedestrian navigation system architecture

3.2.1. Orientation Kalman Filter

The orientation estimation is based on our previous algorithm described in [36], [37] (See Appendix A). This algorithm is a computationally efficient cascaded Kalman filter (CKF) that decouples the tilt (i.e. roll and pitch) Kalman filter and the yaw Kalman filter. This CKF algorithm uses tri-axial accelerometer and gyroscope data for tilt angle estimation in the first step. At the second step, the estimated tilt angles are fused with information from a tri-axial magnetometer and the tri-axial gyroscope to estimate the yaw angle.

The rotation matrix from the sensor frame (s-frame: a coordinate system attached to the inertial sensor) to the navigation frame (n-frame: a local level coordinate system with its x-, y- and z-axis pointing to the East, North and Up direction, respectively), ${}^{n}_{s}R$, is obtained from the orientation Kalman filter and used to estimate the acceleration in the n-frame:

$$\begin{bmatrix} a_{east} \\ a_{north} \\ a_{up} \end{bmatrix} = {}^{n}_{s}R \begin{bmatrix} a_x \\ a_y \\ a_z \end{bmatrix} \tag{3.1}$$

Where $a_{east}, a_{north}\ and\ a_{up}$ are the East, North and Up components of the wrist acceleration; and$a_x, a_y and\ a_z$ are the measured acceleration components from the tri-axial accelerometer.

3.2.2. PCA-based Wrist-swing Direction Estimation

The wrist heading estimation is carried out in a similar fashion to previous works that use Principal Component Analysis (PCA) on a cellphone in a pocket or in multiple carrying mode [38]. The difference is that, in this study, the PCA is applied on wrist acceleration from the smartwatch's sensors to determine its heading direction.

The PCA is applied to every 2-second window of the horizontal acceleration in the n-frame (East and North components of the acceleration). The wrist swing direction is then simply the first eigenvector from the PCA (Figure 3.2). Since the head yaw angle will also be calculated in here, the 180 degree heading ambiguity from the PCA can be easily resolved by finding the closest angle to the head yaw angle.

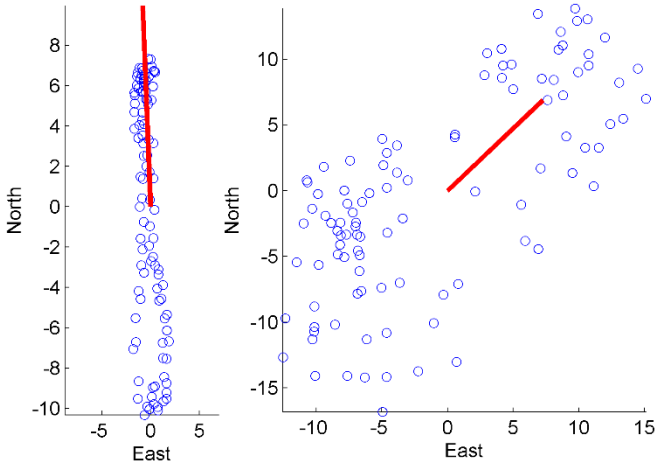

Figure 3.2. PCA wrist-swing direction estimation for walking (left) and running (right)

3.2.3. Step Counter

The step counter uses the smartglasses' tri-axial accelerometer signals. From our observations, using sensors on the head is more robust for step counting than using those on the wrist. This is because the head, while not rigidly connected to the human trunk, exhibits significantly less motion artifacts than the arms. When using a wrist acceleration-based step counter, one has to assume that the cyclic motion is only from walking/running, otherwise a more sophisticated activity classification method that can detect walking and running from other daily activities is desired.

There are a variety of methods to detect steps based on acceleration signals including: windowed peak detection (WPD), hidden Markov model (HMM) and continuous wavelet transform. A previous study in [39] showed that WPD performed as well as other more computationally intensive methods. For the WPD, first, a 3rd order Butterworth filter with a cut-off frequency of 3.5Hz is used to filter out the double spikes. The frequency of 3.5Hz is equivalent 210 steps per minute, which encompasses the standard running cadence of around 180 steps per minute. Then, using peak-counting

with an acceleration threshold of 3m/s2, the number of steps can be accurately detected. The threshold is necessary to ignore the double peaks that are not successfully filtered out, as shown in Figure 3.3.

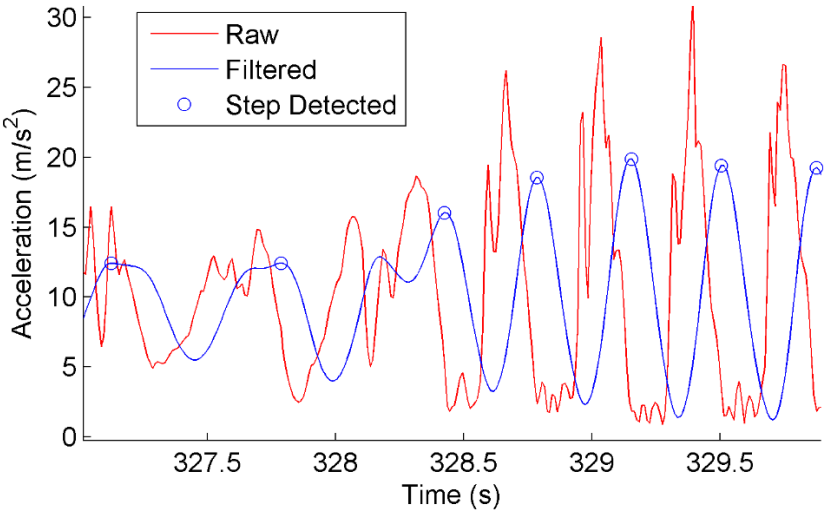

Figure 3.3. Step counter using threshold peak detection

3.2.4. Step Length Estimator

In human gait, there are slight step length variations between steps. In [40], it is shown that by estimating the step length using an accelerometer, the final step distance can be more accurate. There are multiple step length estimation methods available in the literature. In [41], five common methods were compared, and it was suggested that the method that uses the empirical relation of the vertical acceleration [40] performs as well as the rest, while being relatively easy to implement. The step length, S, can then be estimated by:

$$S = K\sqrt[4]{a_{up,max} - a_{up,min}} \tag{3.2}$$

where S is the step length, K is a scalar constant, $a_{up,max}$ is the maximum vertical head acceleration magnitude, and $a_{up,min}$ is the minimum vertical head acceleration magnitude.

In this study, two different step length estimations for walking and running are used, as they have different acceleration signatures. Walking and running can be distinguished with a high accuracy by using the variance of the total acceleration [13].

3.2.5. Head Rotation Detection

The proposed head rotation detection algorithm utilizes the sensors found on both the smartwatch and smartglasses. Using the hand swing direction derived from the PCA in Sec. II.B, the relative changes in the hand swing direction can be used to detect if a user is staying the course or taking a turn.

Based on our observations, head and body rotations differ during walking and running in a few common scenarios, e.g.:

1. ***While walking/running straight, the head stays in neutral position.*** This is the most common scenario, where the user is looking in the direction of walking or running motion. In this scenario, both the head angle and arm swing angle should have relatively small changes in heading.
2. ***While walking/running straight, the head rotates to one side.*** When a user is walking or running, s/he might be looking left or right. In this case, the head angle slope will be either negative or positive, depending if s/he is looking left or right, while the arm swing direction should be relatively constant.
3. ***While walking/running straight, the head rotates from side to side.*** For example, a runner might be checking for traffic on both sides before crossing. In this case, the head angle slope will go from negative to positive or vice-versa, depending if s/he is looking from left to right or from right to left.
4. ***During a turn, the head and body turn at the same time.*** This is similar to Scenario 1, except that both the head and arm swing heading will change at the same time.
5. ***During a turn, the head leads the body into a turn***. Sometimes runners would look into a turn before they turn. In this scenario, the head heading will change followed by the arm swing heading.

6. ***During a turn, the body leads the head into a turn.*** As opposed to Scenario 5, a runner might turn his body first before looking into the new direction. In this case, the arm swing heading will change followed by the head angle.

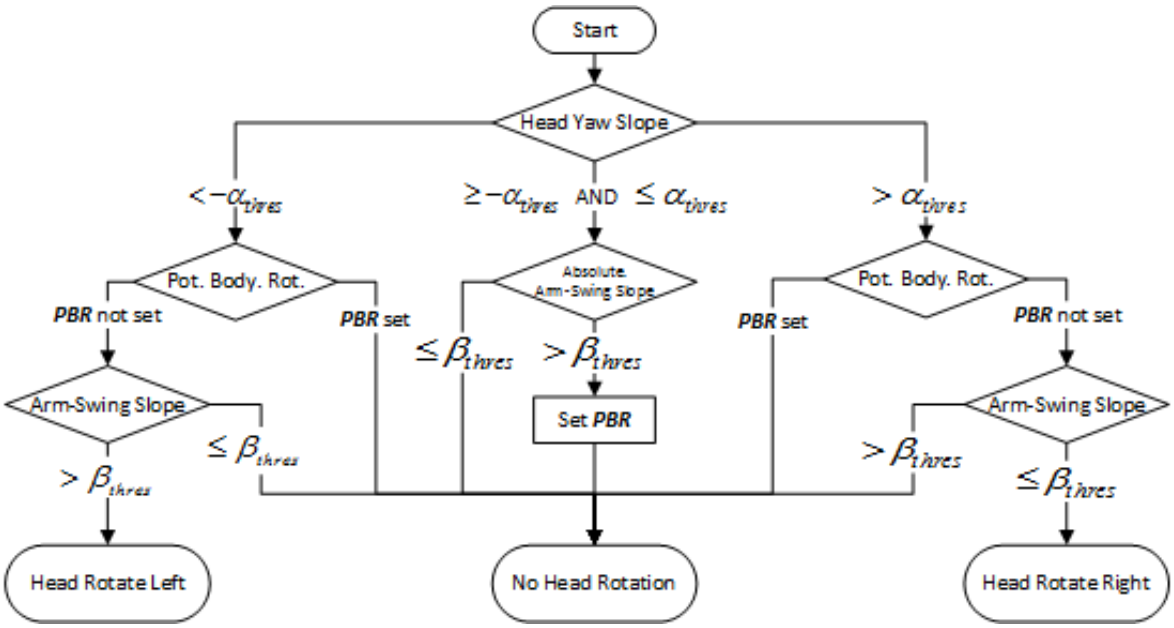

Figure 3.4. Head rotation detection algorithm flowchart

The proposed head rotation detection algorithm shown in Figure 3.4 is used to detect if a user is rotating his/her head. Based on the above six scenarios, whether the head is rotating left or right can be classified based on the head yaw slope, arm swing slope, and potential body rotation (PBR). For every 1s window with 0.5s overlap, the head yaw angle slope is calculated using the orientation KF. Direction of the arm swing is subject to erratic variations due to the nature of unconstrained arm swing motion. Thus, a larger 2s window with 0.5s overlap is used to estimate its corresponding slope in every window. The PBR is a "memory" to keep track of the changes in arm swing slope in the case of Scenario 6, where the user rotates the body prior to rotating the head. It is set when there are changes in the arm swing slope but not in the head yaw slope, and cleared after 2s. The α_{thres} and β_{thres} are the head and body rotation thresholds, in degrees per seconds, respectively. In head rotation motion (Scenarios 2 and 3), α_{thres} will be triggered (e.g., Figure 3.5). When changing direction (Scenarios 4-6), both α_{thres} and β_{thres} will be triggered (e.g., Figure 3.6).

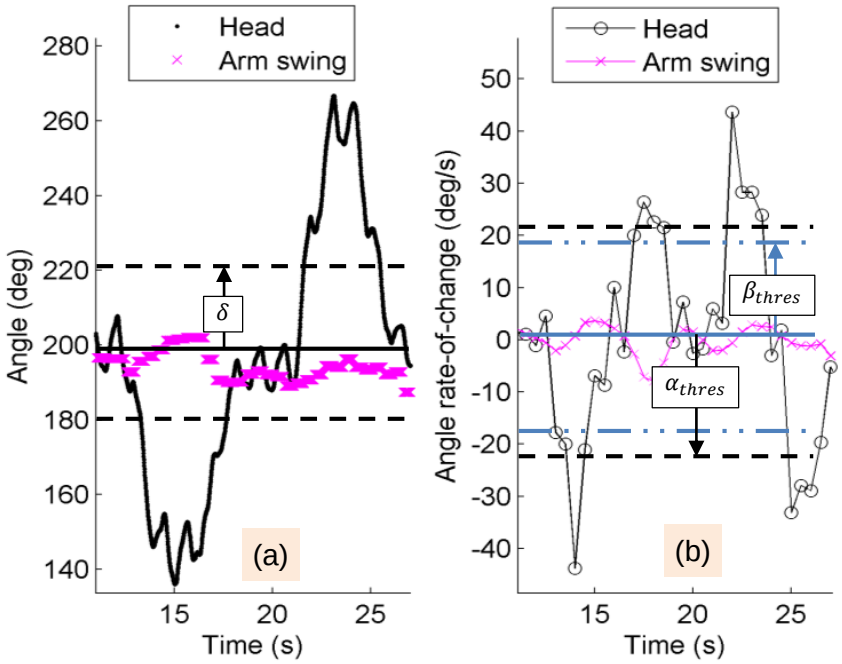

Figure 3.5 **Right and left head rotation while walking (sample): Head yaw angle and arm swing direction (a) and their corresponding rate-of-change (b)**

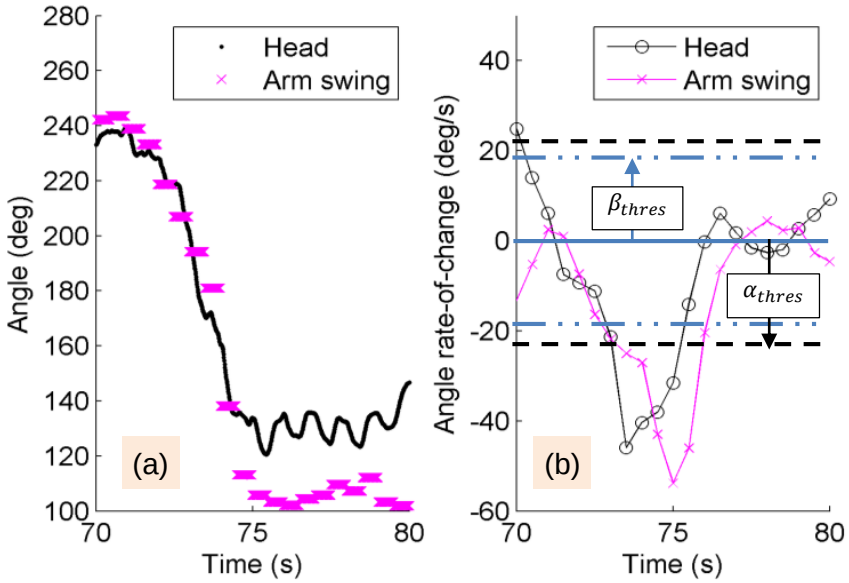

Figure 3.6. **Turning right while walking (sample): Head yaw angle and arm swing direction (a) and their corresponding rate-of-change (b)**

Next, the head's range of motion is divided into the following three states: looking left, forward, or right (see Figure 3.7). A buffer, δ of 20 degrees left and right of the body's medial sagittal plane is set to be the "forward" state; 20 degrees or more right of the medial sagittal plane would be the "right" state; and 20 degrees left of the medial sagittal plane would be the "left" state (Figure 3.6). Then, Delta Last Known Heading (ΔLKH) is the difference between the current head angle, $\psi_{current}$ and the last known forward heading, ψ_{last}:

$$\Delta LKH = \psi_{last} - \psi_{current} \tag{3.3}$$

The last known forward heading, ψ_{last} is the head yaw measured when the active state is "forward". The dash-line in the state diagram is a "fail-safe" logic in case it is stuck in the "left" or "right" state. The assumption is that a user would not be looking left or right for more than 5 seconds while walking or running in normal circumstances.

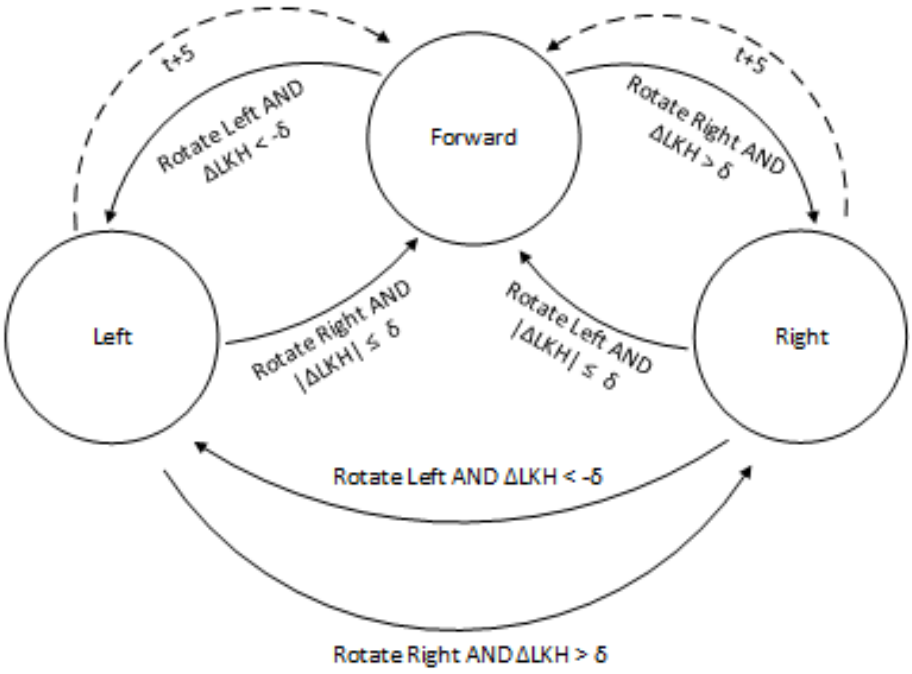

Figure 3.7. Head direction state diagram

3.2.6. Dead Reckoning

The dead reckoning algorithm uses the standard position propagation equation:

$$\begin{cases} p_{lon_k} = p_{lon_{k-1}} + S \cdot \sin\psi_{last} / \lambda_{lon} \\ p_{lat_k} = p_{lat_{k-1}} + S \cdot \cos\psi_{last} / \lambda_{lat} \end{cases} \tag{3.4}$$

where p_{lon_k} is the longitude at time k, p_{lat_k} is the latitude at time k, S is the step length, ψ_{last} is the last known forward heading; λ_{lon} and λ_{lat} are the length of a degree of longitude and latitude, respectively.

The length of a degree of longitude, λ_{lon} and latitude, λ_{lat} on a WGS84 geodetic system for a given latitude, ϕ can be estimated by

$$\begin{cases} \lambda_{lon}(\phi) = \frac{a(1-e^2)}{(1-e^2\sin^2(\phi))^{\frac{3}{2}}} \\ \lambda_{lat}(\phi) = \frac{a\cos(\phi)}{(1-e^2\sin^2(\phi))^{\frac{1}{2}}} \end{cases} \tag{3.5}$$

where a is the equatorial radius, defined exactly as 6378137 meters in WGS84 [42].

3.3. Data Collection

To test the proposed head-wrist PDR, several separate data collection experiments were conducted to examine the performance of each distinct algorithm block (summarized in Table 3.1). Based on Table 3.1, the experimental trials aimed to verify accuracy of the step counting, step length estimation, the proposed head-rotation detection and the head-wrist PDR.

Since the head-turn detection algorithm requires tuning of multiple thresholds, ten subjects were used for that test outlined in Sec. III. C.1. For the step length and

head-wrist PDR test outlined in Sec. III C.2 and C.3, only two subjects were tested as the step length algorithm has been tested in the previous literature [43], while the biggest variable in the Head-Wrist PDR performance is the head-rotation detection.

Table 3.1. Summary of Field Tests Conducted

Test	Location	Subjects
1. Head-turn detection	Various indoor and outdoor locations	10
2. Step-counter and step length	Outdoor track	2
3. Full PDR	Suburb neighborhood	2

3.3.1. Test Subjects

Ten young healthy participants were recruited for the field tests. The only requirement was that they could comfortably run for at least ten minutes. The test subjects consist of nine males and one female, the average age is 27.7±5.2 years old with an average height of 173.2±6.4cm. For the step test and head-wrist PDR test, the two subjects were both male, 28 and 27 years old, 179cm and 165cm, respectively. Prior to the experiment, all the participants agreed and signed the participant consent form approved by Simon Fraser University's Research Ethics Board.

3.3.2. Field Test Equipment

A smartwatch and smartglasses that are readily available on the market were used: LG G Watch R and Recon Jet (Figure 3.8). These wearable devices run customized Android and Android Wear operating systems, respectively. Two custom Android applications were installed to log the sensors data into the internal memory storage. The relevant sensors specifications are listed in Table 3.2 and 3.3.

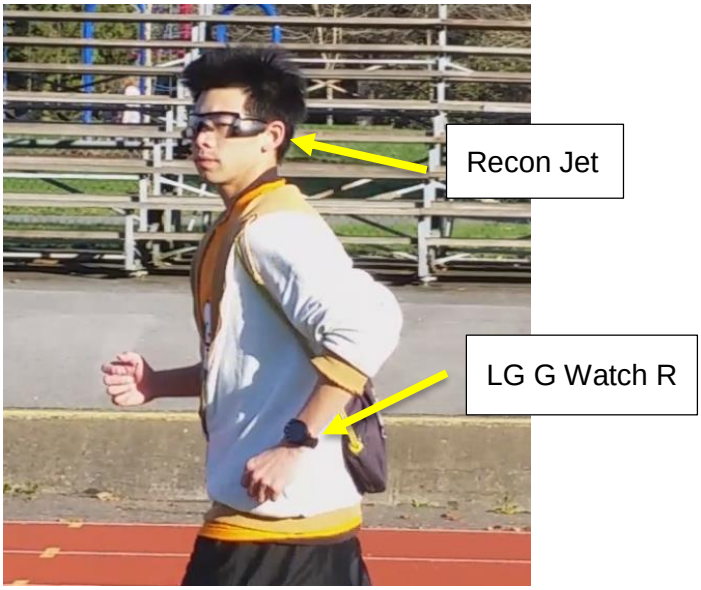

Figure 3.8. A test subject wearing the smartglasses and smartwatch

Table 3.2. Selected Recon Jet Sensors Specifications

Sensor	Accelerometer	Gyroscope	Magnetometer
Part no.	ST LSM9DS0		
Full range	±4g	±2000dps	±400uT
Sensitivity	0.12mg	0.07dps	0.016uT
Date rate	100Hz	100Hz	100Hz

Table 3.3. Selected Lg G Watch R Sensors Specifications

Sensor	Accelerometer	Gyroscope	Magnetometer
Part no.	InvenSense MPU-6515		AKM AK8963
Full range	±2g	±1000dps	±4900uT
Sensitivity	0.061mg	0.03dps	0.15uT
Data rate	50Hz	50Hz	50Hz

3.3.3. Experimental Procedures

Head-turn detection experiment

In order to validate the thresholds α_{thres} and β_{thres} for the head rotation detection algorithm presented in Sec. 3.2.5, the ten participants were asked to perform the six scenarios outlined previously. Each participant was asked to perform the following combination of motion four times while walking and four times while running:

1. Moving straight: look left (slow)
2. Moving straight: look right (slow)
3. Moving straight: look left (fast)
4. Moving straight: look right (fast)
5. Moving straight: look from left to right (slow)
6. Moving straight: look from right to left (slow)
7. Moving straight: look from left to right (fast)
8. Moving straight: look from right to left (fast)
9. Turn left: head-leads-body
10. Turn right: head-leads-body
11. Turn left: body-leads-head
12. Turn right: body-leads-head

The whole experiment was captured in a video for post-experimental video analysis.

Step counter and step length estimation experiment

To test the step counter and step length estimation performance of the algorithm on head-worn sensors, two subjects were asked to perform an outdoor experiment. Using the known distance on a standard Olympic-sized running track, each subject performed the test sequence in Table 3.4 once. To get the reference step counts, the whole experiment was recorded by a video camera. The “ground truth” step counts were obtained by manually counting the steps in post-experimental video analysis.

Table 3.4. Step Count and Step Length Test Sequence

Test sequence	Distance
A) Walk 1 lap	400m
B) Run 1 lap	400m
C) Walk 1 lap followed by run 1 lap	800m
Total distance	**1200m**

Dead reckoning experiment

To test the proposed head-wrist PDR, the same two subjects were asked to walk and run around a block in a suburban neighborhood. Each lap is about 400m, for a total of about 800m. They were instructed to walk and run naturally, and were free to rotate their heads while they ran. Since it is hard to run naturally while carrying a laptop and a survey grade GNSS systems (to provide reference trajectory) in a heavy and bulky backpack, the test subjects were instructed to run as closely to the predefined path as possible.

3.4. Experimental Results and Discussions

The data collected on the smartwatch and smartglasses were analyzed using MATLAB.

3.4.1. Head-turn Detection Test

After counting the total number of head and body turn motions, 36 to 40 head turns and body turn motions, respectively, were recorded from the ten subjects. Using α_{thres} = 25 degree/s and β_{thres} = 20 degree/s, the head rotation motion (motion 1-8 outlined in Sec. III.C-1) results are presented in Table 3.5. The left and right motions are

grouped into a single result because there are no distinctive differences in performance for left and right motions. The detection rate was calculated as

$$Detection\ Rate = \frac{motion\ detected}{motion\ performed} \times 100\% \quad (3.6)$$

For the head rotation test, the worst performance is from single sided head-rotation during walking, with 88.9% detection rate. From our video observation, some subjects have a higher degree of upper body rotation when instructed to look left/right. Thus, the head-turn detection algorithm misclassifies this as course change, since the head and arm-swing heading indicate a change in heading. For running, the head-rotation detections are more successful, with the lowest being 90% for the single-sided head rotation. Again, some subjects were observed to over-rotated their upper body along with their head when they look left, which triggers the false negative outcome.

Table 3.5. Head Rotation Test Results

Activity	**Walking**				**Running**			
Head Rotate	One side		Side to side		One side		Side to side	
Speed	Slow	Fast	Slow	Fast	Slow	Fast	Slow	Fast
Detected	64/72	65/72	67/72	65/72	72/80	76/80	76/80	74/80
Detection Rate	88.9%	90.3%	93.1%	90.3%	90%	95%	95%	92.5%

The results for the course change test (motion 9-12 outlined in Sec. III.C-1) are presented in Table 3.6. For the course change test, it is more accurate to describe a successful detection as *not* detecting any head turns (false positives) due to turning motion. The head-leads-body turn while walking shows the worse performance with 90.6% detection rate. This is caused by the delay in the arm swing direction change after the head rotation, or the arm swing direction change is not as abrupt as the body-leads-head turn or full-body turn. For the body-leads-head turn, the performance is excellent with 98.4% detection rate. Less delay is observed in the body-leads-head turns than the head-leads-body turns. Some subjects found this motion awkward and unnatural for

walking turns. For running, all course changes are detected, be it head-leads-body or body-leads-head. This is because running turns are usually more abrupt than walking, so it is much easier to detect the change in direction for both head and arm swings.

Table 3.6. Course Change Test Results

Activity	Walking		Running	
Style	Head lead	Body lead	Head lead	Body lead
Detected	58/64	63/64	72/72	72/72
Detection Rate	90.6%	98.4	100%	100%

3.4.2. Step counter and Step length estimation test

The step count test results are shown in Table 3.7. For step detection, the head-worn sensors show excellent performance with an error less than 0.36%. There is no noticeable variation in step count accuracy between running and walking.

Table 3.7. Step Count Test Results

Step Count Trial		Est.	Actual	Error %
a) Walk	Subject 1	571	573	0.35%
	Subject 2	561	559	0.36%
b) Run	Subject 1	347	346	0.29%
	Subject 2	333	334	0.30%
c) Walk + run	Subject 1	899	901	0.22%
	Subject 2	875	877	0.23%

For the step length test, the walking lap (Trial A) and the running lap (Trial B) were used to train the K parameter in Eq. (2). Then, the step length estimation was tested in Trial C: the walking lap followed by a running lap. The results are shown in Table 3.8. With the known distance of 800m (2×400m), the error is less than 19m, or 2.36%.

Table 3.8. Step Length Test Results

800m Track Test		
	Subject 1	**Subject 2**
Cumulative distance	781.13m	788.26m
Error %	2.36%	1.47%

To visualize the step length estimation test in Trial C, the walking and running trajectories are plotted on a Google map for Subjects 1 (Figure 3.9) and 2 (Figure 3.10).

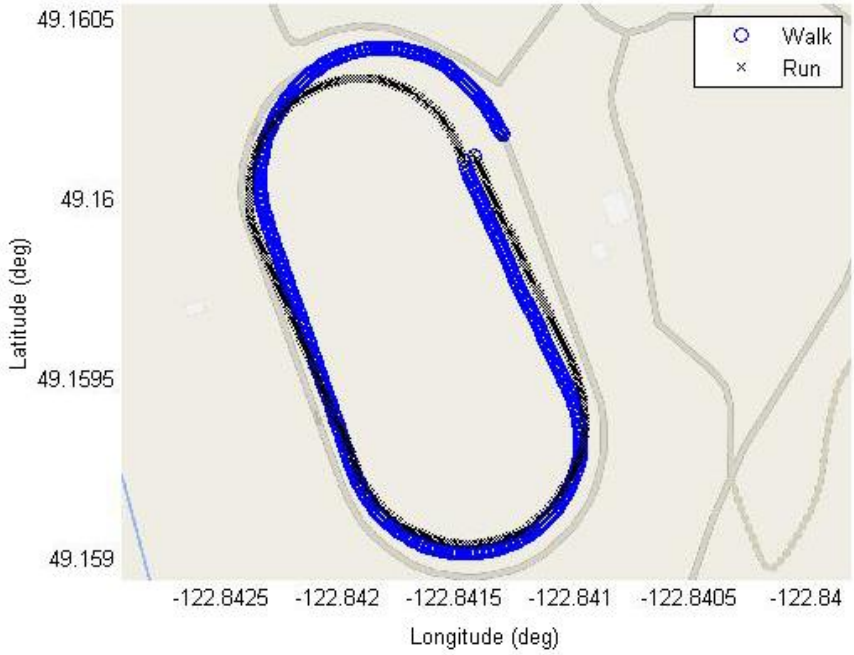

Figure 3.9. Dead reckoning on test track for walking and running (Subject 1)

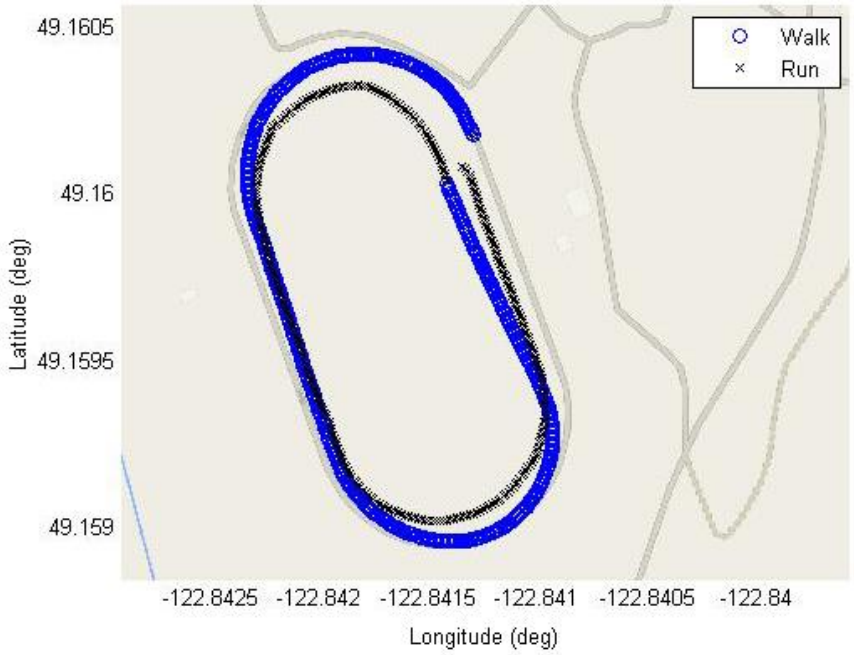

Figure 3.10. Dead reckoning on test track for walking and running (Subject 2)

3.4.3. Dead Reckoning Test

The results for the head-wrist PDR test for two subjects are plotted on Google Map to show how it deviates from actual trajectories. For comparison, the dead reckoning performance using heading derived from head yaw, arm swing angle and head-wrist PDR with head-rotation detection are shown in Figure 3.11-3.13.

As shown in Figure 3.11, the effect of unaccounted head-rotation can skew the dead reckoning position propagation towards the direction of the head turn. Note that in this test, the test subjects rotated their head right followed by left, so the final absolute position does not drift much as opposed to multiple left or multiple right head rotation in succession.

For comparison, the dead reckoning solution obtained using arm swing angle is also plotted in Figure 3.12. For walking, the arm swing heading produced a solution that is reasonable, with little offset from direction of motion. It is more noticeable in running that the arm swing derived heading angles have a larger offset from direction of motion. This is observable in running dynamics, where the arm swing often crosses the front of the body, at an angle from the direction of motion.

Finally, by combining the sensors on the smartglasses and smartwatch, the head rotation can be detected, and the head yaw derived heading at those instances can be discarded. In Fig 3.13, it shows that the performance of the head-wrist PDR heading is similar to the head-only PDR in Figure 3.11, with those position propagation errors caused by head rotation being smoothed out.

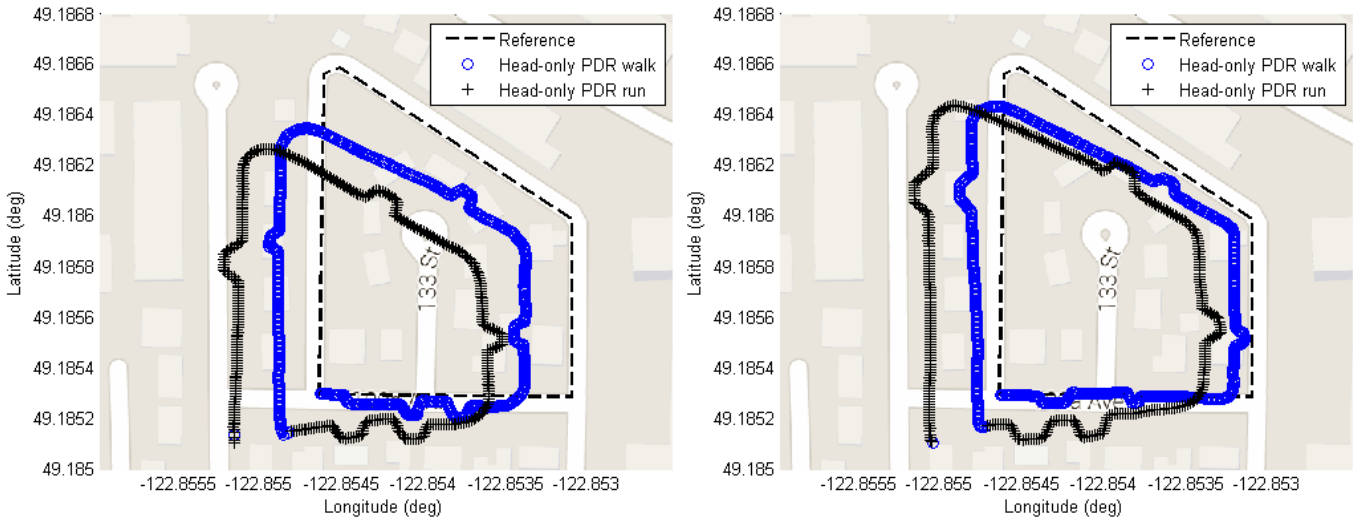

Figure 3.11. Full test with head-only PDR: Subject 1 (left) and subject 2 (right)

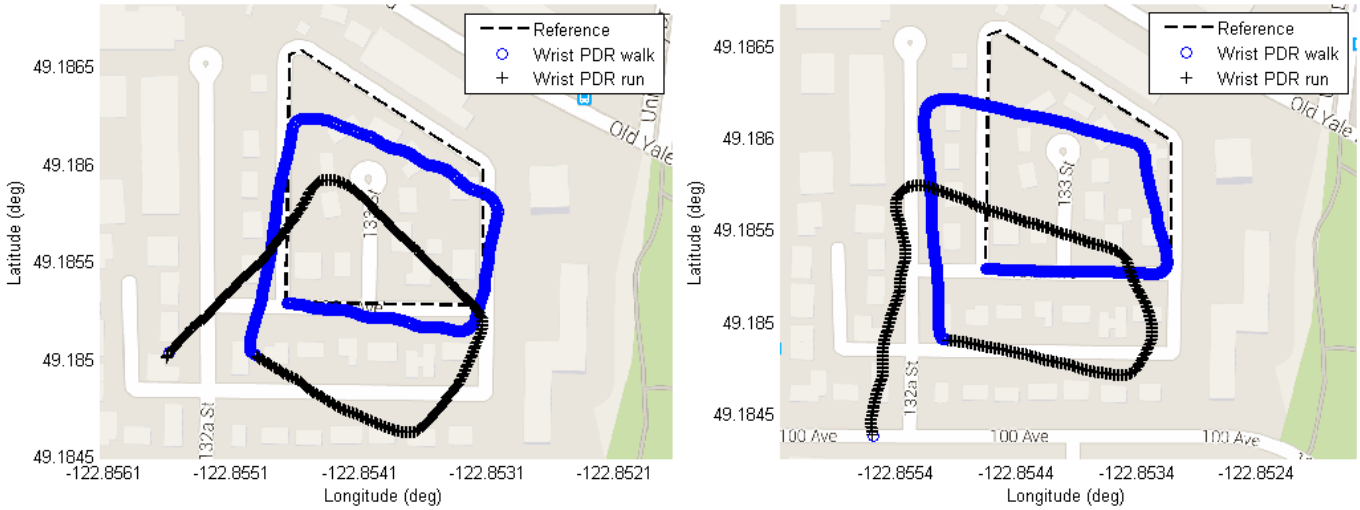

Figure 3.12. Full test with wrist-only PDR: Subject 1 (left) and subject 2 (right)

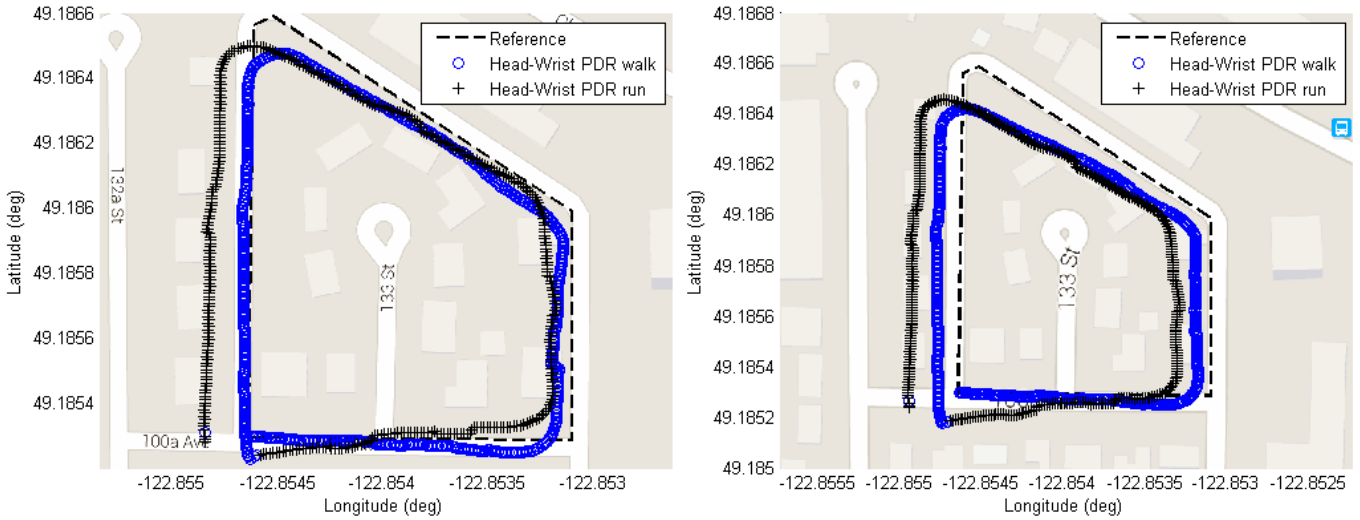

Figure 3.13. Full test with the proposed head-wrist PDR: Subject 1 (left) and subject 2 (right)

The head yaw, arm swing derived heading and the head-wrist PDR heading are plotted in Figure 3.14 and Figure 3.15 for Subjects 1 and 2, respectively. The head rotation periods are successfully detected and the last known forward heading is used as heading over these periods. From Figure 3.14 and 3.15, it can be seen that the wrist swing angles are relatively stable for walking, but are considerably more erratic during running.

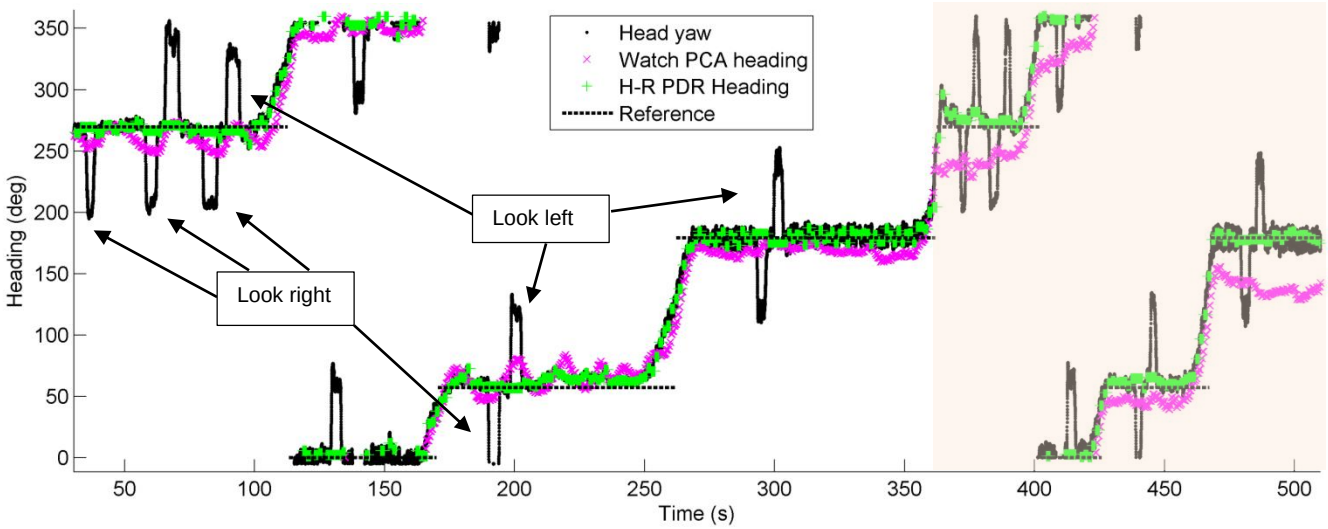

Figure 3.14. Full test head yaw angle of walking and running (shaded) for Subject 1.

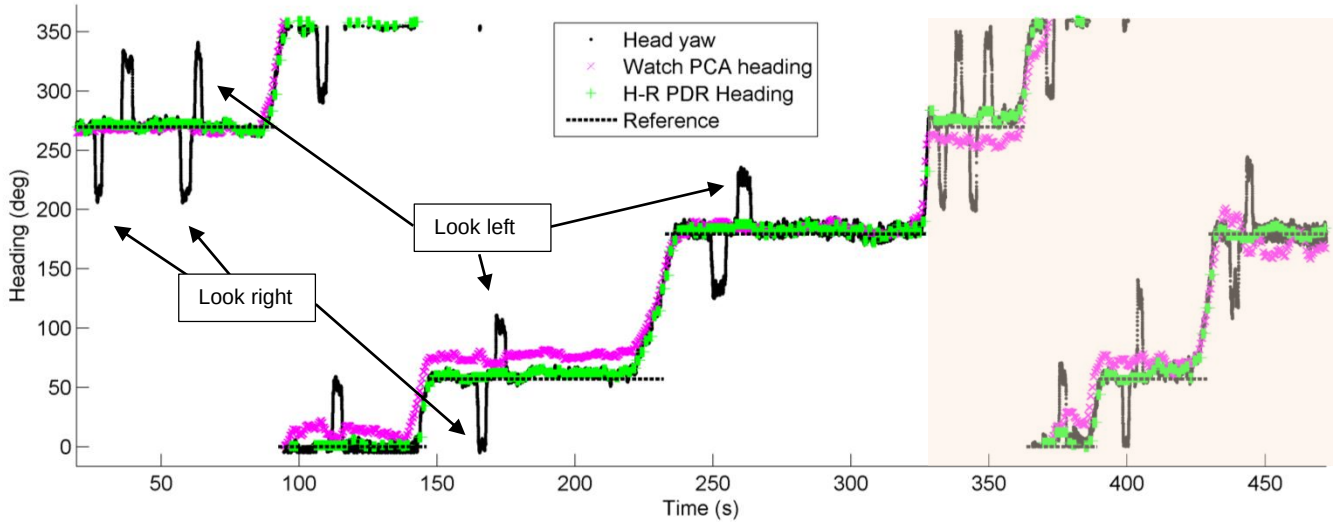

Figure 3.15. Full test head yaw angle of walking and running (shaded) for Subject 2

3.5. Practical Implementation and Limitations

The limitations of this study are related to a few assumptions that are made. It is assumed that the user would only move forward with every step, never in-place,

backwards or sideways. It is also assumed that the user would only look left or right, not 180 degrees backwards. Additionally, the user is expected to have a regular arm swing motion while walking and running. The current proposed algorithm also do not account for when the users put their hands in their pockets, holding something in their hand. However, with a more specialized application, such as for competitive running, these are valid assumptions. In future works, machine learning techniques can be implemented to detect regular arm swing motion to relax the assumption of the hand motion.

In terms of practical implementation in wearable devices, the proposed algorithm is not computationally intensive. The orientation KF is computational efficient and performs well at 50Hz; the PCA and slope estimation for smartglasses and smartwatches can be computed every 0.5s. For data communication between these devices, they provide Bluetooth low energy (BLE) connectivity. In the particular combination of Recon Jet and LG G Watch R used in this study, the former would be chosen as the central processor. The smartwatch can transmit its PCA derived heading to the smartglasses at every 0.5s using BLE, with the main algorithm running on the latter.

3.6. Conclusion

This chapter presents a complete inertial pedestrian dead reckoning (PDR) system targeting walkers and runners using both a smartwatch and smartglasses. The shortcomings of using only the smartwatch or the smartglasses alone for PDR are shown in this study. For the smartglasses, the PDR trajectory is affected by unaccounted head-rotation, while arm swing derived heading does not work as well for running. By combining both types of wearable devices, head-rotation can be detected and correct the heading appropriately. The results show that it is highly feasible to fuse the smartwatch and smartglasses data in an inertial dead reckoning system that would otherwise be hard to implement on just a smartwatch or smartglasses alone.

Chapter 4.

Conclusion

In this concluding chapter, each chapter is be summarized, followed by discussions of practical implementation of the proposed methods. Finally, this thesis ends with recommendations and ideas for future works.

4.1. Thesis Summary and Conclusion

In this thesis, sensors fusion from multiple wearable sensors are proposed for human activity recognition (HAR) and pedestrian dead reckoning (PDR).

Chapter 1 introduces the popularity of wearable devices and its potential growth. The immense benefits of HAR and PDR research and its state-of-the-art literature are also introduced. These factors motivate the research direction presented in this thesis.

Chapter 2 presents a novel method to classify fitness activities using head-worn accelerometer, barometric pressure sensor and GPS, with comparisons to other common mounting locations on the body. Using multiclass SVM on head-worn sensors, an average F-score of 96.66% is obtained for classifying standing, walking, running, ascending/descending stairs and cycling. The best sensor location combinations were found to be on the ankle plus another upper body location. Using three or more sensors did not show a notable improvement over the best two-sensor combinations.

In **Chapter 3**, a complete inertial dead reckoning solution that includes step detection, step length estimation, head-rotation detection, and dead reckoning using a smartwatch and smartglasses that are currently available in the market is presented. By using arm swing direction from smartwatch and head yaw angle from smartglasses, head rotation can be detected. With this knowledge, the head-based PDR can distinguish between head yaw angle and true direction of motion. Using the smartglasses, step detection with an error rate less than 2.36% and a cumulative distance error of less than 2.36% on 800m walks and runs is achieved. In the dead reckoning field experiments, the proposed algorithm produces result that closely track the actual path when plotted on Google map, outperforming solutions that only use the smartwatch or smartglasses alone.

4.2. Practicality of Proposed Algorithms

The research presented in this thesis is motivated by the abundance of wearable devices currently available in the market. Therefore, the practicality of actual implementation of the proposed HAR and PDR algorithms is important.

For the sake of discussions, the wearable devices listed in Table 4.1 are used as basis of implementation discussion. These devices run Android-based operating system. Android is a java-based application development platform. However, the Android SDK supports the use of native C/C++ to maximize computational speed using NDK (Native Development Kit).

Table 4.1. Selected Wearable Devices Technical Specs.

Worn location	Wearable Device	Tech. Specs.	Connectivity
Head	Google Glass	Dual-core 1GHz ARM Cortex-A9 1 GB RAM	Bluetooth 4.0 Wi-Fi
	Recon Jet	Dual-core 1GHz ARM Cortex-A9 1 GB RAM	Bluetooth 4.0 Wi-Fi
Wrist	Samsung Gear Live	Quad-core 1.2GHz Cortex-A7 512 MB RAM	Bluetooth 4.0 Wi-Fi
	LG G Watch R	Quad-core 1.2GHz Cortex-A7 512 MB RAM	Bluetooth 4.0 Wi-Fi

In the proposed HAR method, it is shown that by just using head-worn sensors, fitness activities can be accurately classified with an average F-score of 96.66%. Since only 16 features are being used, the corresponding SVM operation is done in a pretty small scale. The SVM model can even be trained offline, and using the trained model for testing. Chapter 2 also showed that using 3 or more combination sensors does not show noticeable improvement over 2-sensors combination. In that case, the slower of the two wearable devices, the “slave” will send the sensors data to the more powerful device, the “master”. The SVM classifier will be ran on the “master” device. The head-worn devices like Google Glass and Recon Jet have more powerful processor, they are suitable to be the “master” while the smartwatches are the “slave”. Since they all have Bluetooth 4.0 connectivity, that would be ideal for inter-device communication.

For the proposed PDR algorithm, the most complex operation would be the orientation Kalman filter. However, the proposed algorithm uses a decoupled Kalman filter that reduces the complexity of matrix inversion in the Kalman filter. A similar “master” and “slave” devices configuration can be used for the head-wrist PDR.

However, one drawback of the implementations is the power consumption of required for the continual processing, sensors operation and device connectivity. These wearable devices have considerably smaller battery capacity, as compared to a standard smartphone. However, as wearable devices become more power efficient and employ larger battery capacity, this problem will be minimized.

4.3. Future Works

The HAR and PDR algorithms proposed are built on some basic assumptions and limitations. This section discusses some potential ideas for future works that can mitigate these assumptions and limitations.

4.3.1. Combined HAR and PDR

Since pedestrian dead reckoning is ultimately only valid for human locomotion, the HAR can be used as a pre-requisite to the PDR algorithm. By combining the proposed HAR and PDR, in which the PDR will only be activated when walking, running, ascending /descending stairs, the PDR will not be running in other non-valid activities such as cycling.

4.3.2. Aided PDR System

Inertial dead reckoning solutions will drift over long period of time, even when using tactical grade IMUs with accurate sensor modeling. The proposed PDR system can be combined with absolute positioning solutions like GNSS or Wi-Fi to achieve aided-PDR navigation. Inherently, GPS is also available in Recon Jet, as well as many fitness oriented wearable devices. A low-cost GPS-Inertial Navigation System can be implemented in these device combinations. For indoor localization, Wi-Fi and BLE are commonly available in the latest wearable devices.

4.3.3. Expanded activities recognition

Six fitness activities are classified using the proposed HAR – standing, walking, running, ascending/descending stairs and cycling. Other popular fitness activities such as inline skating, indoor cycling, and rowing can be included in future work.

4.3.4. Self-annotate HAR data collection

In this thesis, the proposed HAR algorithm is only trained and tested on 8 test subjects. The data collection is time consuming due to the need to review video footage and tag the activities accordingly. However, most wearable devices nowadays support user-written applications. Custom apps can be written for a self-reporting data collection. Test participants just have to manually annotate their current activities in the app. This can pave the way for longitudinal data collection with a large number of subjects.

References

[1] "Wearable Technology Future is Ripe for Growth – Most Notably among Millennials, Says PwC US," *PricewaterhouseCoopers*, 2014. [Online]. Available: http://www.pwc.com/us/en/press-releases/2014/wearable-technology-future.html. [Accessed: 18-Jan-2016].

[2] *Racing toward a complete digital lifestyle : Digital Consumers Crave More Accenture Digital consumer crave more.* New York: Accenture, 2014.

[3] G. Tudela, K. Mackenzie, and P. Telfer, "WEARABLE TECH MARKET," *Vandrico, Inc*, 2016. [Online]. Available: http://vandrico.com/wearables/. [Accessed: 31-Jan-2016].

[4] O. D. Lara and M. A. Labrador, "A Survey on Human Activity Recognition using Wearable Sensors," *IEEE Commun. Surv. Tutorials*, vol. 15, no. 3, pp. 1192–1209, 2013.

[5] A. Bulling, U. Blanke, and B. Schiele, "A tutorial on human activity recognition using body-worn inertial sensors," *ACM Computing Surveys*, vol. 46, no. 3, pp. 33:1-33:33, 2014.

[6] S. Beauregard, "A helmet-mounted pedestrian dead reckoning system," *3rd Int. Forum on Appl. Wearable Comput.(IFAWC)*, Bremen, Germany, Mar. 15-16, 2006.

[7] L. Fang, P. J. Antsaklis, L. a. Montestruque, M. B. McMickell, M. Lemmon, Y. Sun, H. Fang, I. Koutroulis, M. Haenggi, M. Xie, and X. Xie, "Design of a wireless assisted pedestrian dead reckoning system - The NavMote experience," *IEEE Trans. Instrum. Meas.*, vol. 54, no. 6, pp. 2342–2358, 2005.

[8] R. Harle, "A Survey of Indoor Inertial Positioning Systems for Pedestrians," *IEEE Commun. Surv. Tutorials*, vol. 15, no. 3, pp. 1281–1293, 2013.

[9] L. Bao and S. S. Intille, “Activity Recognition from User-Annotated Acceleration Data,” *Pervasive Comput.*, vol. 3001, pp. 1 – 17, 2004.

[10] S. Ishimaru, K. Kunze, and K. Kise, “In the Blink of an Eye – Combining Head Motion and Eye Blink Frequency for Activity Recognition with Google Glass,” *Proc. 5th Int. Conf. of Augmented Human,* Kobe, Japan, Mar. 7-9, 2014.

[11] B. Lo, L. Atallah, O. Aziz, M. El Elhew, A. Darzi, and G. Yang, “Real-Time Pervasive Monitoring for Postoperative Care,” *Proc. 4th Int. Work. Wearable Implant. Body Sens. Networks (BSN 2007)*, Aachen, Germany, Mar. 26-28, 2007.

[12] L. Atallah, B. Lo, R. King, and G. Z. Yang, “Sensor positioning for activity recognition using wearable accelerometers,” *IEEE Trans. Biomed. Circuits Syst.*, vol. 5, no. 4, pp. 320–329, 2011.

[13] P. Anastasopoulou, M. Tansella, J. Stumpp, L. Shammas, and S. Hey, “Classification of human physical activity and energy expenditure estimation by accelerometry and barometry,” *Proc. 34th Int. Conf. of IEEE Eng. Med. Biol. Soc. (EMBC),* San Diego, CA, Aug. 28-Sept. 1, 2012.

[14] O. Mezentsev, G. Lachapelle, and J. Collin, “Pedestrian Dead Reckoning - A Solution to Navigation in GPS Signal Degraded Areas?,” *Geomatica*, vol. 59, no. 2, pp. 175 – 182, 2005.

[15] M. E. C. S. Godha, G. Lachapelle, “Integrated GPS/INS System for Pedestrian Navigation in a Signal Degraded Environment,” *Proc. 19th Int. Tech. Meet. Satell. Div. Inst. Navig. (ION GNSS)*, Fort Worth, TX, Sept. 26-29, 2006.

[16] Y. Zhuang and N. El-Sheimy, “Tightly-Coupled Integration of WiFi and MEMS Sensors on Handheld Devices for Indoor Pedestrian Navigation,” *IEEE Sens. J.*, vol. 16, no. 1, pp. 224–234, 2016.

[17] F. Evennou and F. Marx, “Advanced integration of WiFi and inertial navigation systems for indoor mobile positioning,” *EURASIP J. Appl. Signal Processing*, vol. 2006, pp. 1–11, 2006.

[18] S. Zihajehzadeh, P. K. Yoon, B. Kang, and E. J. Park, “UWB-Aided Inertial Motion Capture for Lower Body 3-D Dynamic Activity and Trajectory Tracking,” *IEEE Trans. Inst. Meas.*, vol. 64, no. 12, pp. 3577–3588, 2015.

[19] M. Kok, J. Hol, and T. Schon, “Indoor positioning using ultra-wideband and inertial measurements,” *IEEE Trans. Veh. Technol.*, vol. 64, no. 4, pp. 1293–1303, 2015.

[20] C. Fischer, K. Muthukrishnan, M. Hazas, and H. Gellersen, “Ultrasound-aided pedestrian dead reckoning for indoor navigation,” *Proc. 1st ACM Int. Work. Mob. Entity Localization Track. GPS-less Environ. (MELT)*, San Francisco, CA, Sept 19, 2008.

[21] H. Bao and W.-C. Wong, “A Novel Map-Based Dead-Reckoning Algorithm for Indoor Localization,” *J. Sens. Actuator Networks*, vol. 3, no. 1, pp. 44–63, 2014.

[22] E. Foxlin, “Pedestrian tracking with shoe-mounted inertial sensors,” *IEEE Comput. Graph. Appl.*, vol. 25, no. 6, pp. 38–46, 2005.

[23] M. Dippold, “Personal dead reckoning with accelerometers,” Proc. 3rd *Int. Forum on Appl. Wearable Comput. (IFAWC),* Bremen, Germany, Mar. 15-16, 2006.

[24] P. Goyal, V. J. Ribeiro, H. Saran, and A. Kumar, “Strap-down Pedestrian Dead-Reckoning system,” *Proc. Int. Conf. Indoor Position. Indoor Navig. (IPIN)*, Guimaraes, Portugal, Sept. 21-23, 2011.

[25] R. Jirawimut, P. Ptasinski, V. Garaj, F. Cecelja, and W. Balachandran, “A method for dead reckoning parameter correction in pedestrian navigation system,” *IEEE Trans. Instrum. Meas.*, vol. 52, no. 1, pp. 209–215, 2003.

[26] B. Cinaz and H. Kenn, “Head SLAM - Simultaneous localization and mapping with head-mounted inertial and laser range sensors,” *Proc. 12th Int. Symp. Wearable Comput. (ISWC),* Pittsburg, PA, Sept. 28-Oct. 1, 2008.

[27] M. Baglietto, A. Sgorbissa, D. Verda, and R. Zaccaria, “Human navigation and mapping with a 6DOF IMU and a laser scanner,” *Rob. Auton. Syst.*, vol. 59, no. 12, pp. 1060–1069, 2011.

[28] S. H. Collins, P. G. Adamczyk, and A. D. Kuo, “Dynamic arm swinging in human walking,” *Proc. R. Soc. B Biol. Sci.*, vol. 276, no. 1673, pp. 3679–3688, 2009.

[29] S. M. Bruijn, O. G. Meijer, P. J. Beek, and J. H. van Dieen, “The effects of arm swing on human gait stability,” *J. Exp. Biol.*, vol. 213, no. 23, pp. 3945–3952, 2010.

[30] D. Simon, *Optimal State Estimation: Kalman, H Infinity, and Nonlinear Approaches*. New York: Wiley, 2006.

[31] S. Zihajehzadeh, T. J. Lee, J. K. Lee, R. Hoskinson, and E. J. Park, “Integration of MEMS inertial and pressure sensors for vertical trajectory determination,” *IEEE*

Trans. Instrum. Meas., vol. 64, no. 3, pp. 804–814, 2015.

[32] M. A. Hearst, S. T. Dumais, E. Osman, J. Platt, and B. Scholkopf, “Support vector machines,” *IEEE Intell. Syst.*, vol. 13, no. 4, pp. 18–28, Jul. 1998.

[33] C. M. Bishop, *Pattern Recognition and Machine Learning*, New York: Springer, 2006.

[34] C. Chang and C. Lin, “LIBSVM : A Library for Support Vector Machines,” *ACM Trans. Intell. Syst. Technol.*, vol. 2, pp. 1–39, 2011.

[35] P.-N. Tan, M. Steinbach, and V. Kumar, *Introduction to Data Mining*. Boston, MA: Addison-Wesley, 2005.

[36] S. Zihajehzadeh, D. Loh, M. Lee, R. Hoskinson, and E. J. Park, “A Cascaded Two - Step Kalman Filter for Estimation of Human Body Segment Orientation Using MEMS - IMU,” *Proc. 36th Annu. Int. Conf. IEEE Eng. Med. Biol. Soc. (EMBC)*, Chicago, IL, Aug. 26-30, 2014.

[37] S. Zihajehzadeh, D. Loh, T. J. Lee, R. Hoskinson, and E. J. Park, “A cascaded Kalman filter-based GPS/MEMS-IMU integration for sports applications,” *Measurement*, vol. 73, pp. 200–210, 2015.

[38] J. Qian, L. Pei, J. Ma, R. Ying, and P. Liu, “Vector Graph Assisted Pedestrian Dead Reckoning Using an Unconstrained Smartphone,” *Sensors*, vol. 15, no. 3, pp. 5032–5057, 2015.

[39] A. Brajdic and R. Harle, “Walk detection and step counting on unconstrained smartphones,” in *Proc. 1st ACM Int. Joint Conf. Pervasive and Ubiquitous Computing (UbiComp),* Zurich, Switzerland, Sept 8-12*,* 2013.

[40] H. Weinberg, “Using the ADXL202 in pedometer and personal navigation applications,” *Analog devices AN-602 Appl. note*, pp. 1–8, 2002.

[41] D. Alvarez, R. C. González, A. López, and J. C. Alvarez, “Comparison of step length estimators from weareable accelerometer devices,” *Proc. 28th Annu. Int. Conf. IEEE Eng. Med. Biol. Soc. (EMBC)*, New York City, NY, Aug 30-Sept. 3, 2006.

[42] J. Farrell, *Aided Navigation: GPS with High Rate Sensors*. New York: McGraw-Hill, Inc., 2008.

[43] I. Apostolopoulos, D. S. Coming, and E. Folmer, “Accuracy of Pedometry on a Head-mounted Display,” *Proc. 33rd Annu. ACM Conf. on Human Factors in Computing Systems (CHI),* Seoul, Korea, Apr. 18-23*,* 2015.

Appendix A.

Cascaded Orientation Kalman Filter

This section summarizes the cascaded orientation Kalman filter from [36]. This is a two-step Kalman filter that decouples the tilt (roll/pitch) and yaw from a traditional central Kalman filter. The orientation of the sensor frame with respect to navigation frame (East, North and up) can be represented by a rotation matrix:

$$^{\mathrm{N}}\mathbf{X}={}^{\mathrm{N}}_{\mathrm{S}}\mathbf{R}\,{}^{\mathrm{S}}\mathbf{x} \tag{A.1}$$

where $\mathbf{x}$ is an arbitrary 3×1 vector and left superscripts N and S represent the navigation and sensor frame respectively. ${}^{\mathrm{N}}_{\mathrm{S}}\mathbf{R}$ is a 3×3 matrix expressed as:

$${}^{\mathrm{N}}_{\mathrm{S}}\mathbf{R}=\begin{bmatrix} c\alpha c\beta & c\alpha s\beta s\gamma - s\alpha c\gamma & c\alpha s\beta c\gamma + s\alpha s\gamma \\ s\alpha c\beta & s\alpha s\beta s\gamma + c\alpha c\gamma & s\alpha s\beta c\gamma - c\alpha s\gamma \\ -s\beta & c\beta s\gamma & c\beta c\gamma \end{bmatrix} \tag{A.2}$$

where c and s are abbreviations for cos and sin respectively; α (yaw), β (pitch), γ (roll) are the rotation angles about the Z-, Y- and X- axes of the navigation frame respectively.

Tilt Kalman Filter

The Tilt Kalman filter uses the following system model equations:

$$\mathbf{x}_1(k)=\mathbf{A}_1(\mathrm{k}-1)\mathbf{x}_1(\mathrm{k}-1)+\mathbf{w}_1(\mathrm{k}-1) \tag{A.3}$$

$$\mathbf{z}_1(k)=\mathbf{C}_1(\mathrm{k})\mathbf{x}_1(\mathrm{k})+\mathbf{v}_1(\mathrm{k}) \tag{A.4}$$

where $\mathbf{x}_1=[-s\beta \quad c\beta s\gamma \quad c\beta c\gamma]$ is the state vector, $\mathbf{A}_1$ is the state transition matrix, $\mathbf{C_1}$ is the observation matrix. $\mathbf{w}_1$ and $\mathbf{v}_1$ are the process model noise and measurement noise model respectively. These matrices in (A.3) and (A.4) can be calculated using the following equations:

$$\mathbf{A}_1(\mathrm{k}-1)=\mathbf{I}_3-\Delta\mathrm{t}\,\tilde{\mathbf{y}}_{\mathrm{G}}(\mathrm{k}-1) \tag{A.5}$$

$$\mathbf{w}_1(\mathrm{k}-1)=\Delta\mathrm{t}\left(-\tilde{\mathbf{x}}_1(\mathrm{k})\right)\mathbf{n}_{\mathrm{G}} \tag{A.6}$$

$$\mathbf{C}_1(\mathrm{k})=\mathrm{g}\mathbf{I}_3 \tag{A.7}$$

$$\mathbf{v}_1(\mathrm{k})={}^{\mathrm{S}}\mathbf{a}^{-}_{\epsilon}(\mathrm{k})+\mathbf{n}_{\mathrm{A}} \tag{A.8}$$

$${}^{\mathrm{S}}\mathbf{a}^{-}_{\epsilon}(\mathrm{k})={}^{\mathrm{S}}\mathbf{a}^{-}(\mathrm{k})+{}^{\mathrm{S}}\mathbf{a}(\mathrm{k}) \tag{A.9}$$

$${}^{\mathrm{S}}\mathbf{a}^{-}(\mathrm{k})=\mathrm{c_a}\,{}^{\mathrm{S}}\mathbf{a}^{+}(\mathrm{k}-1) \tag{A.10}$$

where $\tilde{\mathbf{y}}_{\mathrm{G}}$ is the 3×3 skew-symmetric matrix of tri-axial gyroscope measurements and $\tilde{\mathbf{x}}_1$ is the skew-symmetric matrix of $\mathbf{x_1}$. $\mathbf{I}_3$ is the 3×3 identity matrix. ${}^{\mathrm{S}}\mathbf{a}_{\epsilon}^{-}$ is the external acceleration error in sensor frame and ${}^{\mathrm{S}}\mathbf{a}$ is the acceleration measurement from the accelerometer. The superscripts $+$ and $-$ represents the *a posteriori* and *a priori* estimates in the Kalman filter. $\mathbf{n}_{\mathrm{G}}$ and $\mathbf{n}_{\mathbf{A}}$ are the gyroscope and accelerometer measurement noise and are assumed to be uncorrelated, zero-mean white Gaussian. $0 \leq c_a \leq 1$ is a dimensionless constant and g is the gravity constant. Once all these matrices are calculated, the Kalman filter is process with the following steps:

Step 1: compute the *a priori* state estimates:

$$\mathbf{x}_1^-(k) = \mathbf{A}_1(\mathrm{k}-1)\mathbf{x}_1^+(k-1) \tag{A.11}$$

Step 2: compute the *a priori* error covariance matrix:

$$\mathbf{P}^-(\mathrm{k}) = \mathbf{A}_1(\mathrm{k}-1)\mathbf{P}^+(\mathrm{k}-1)\mathbf{A}_1^{\mathrm{T}}(\mathrm{k}-1) + \mathbf{Q}_1(\mathrm{k}-1) \tag{A.12}$$

where $\mathbf{Q}_1(\mathrm{k}-1) = \mathrm{E}\left[\mathbf{w}_1(\mathrm{k}-1)\mathbf{w}_1^{\mathrm{T}}(\mathrm{k}-1)\right]$ is the process noise covariance matrix.

Step 3: compute the Kalman gain:

$$\mathbf{K}(\mathrm{k}) = \mathbf{P}^-(\mathrm{k})\mathbf{C}_1^{\mathrm{T}}(\mathrm{k})\left[\mathbf{C}_1(\mathrm{k})\mathbf{P}^-(\mathrm{k})\mathbf{C}_1^{\mathrm{T}}(\mathrm{k}) + \mathbf{R}_1(\mathrm{k})\right]^{-1} \tag{A.13}$$

where $\mathbf{R}_1(\mathrm{k}) = \mathrm{E}\left[\mathbf{v}_1(\mathrm{k})\mathbf{v}_1^{\mathrm{T}}(\mathrm{k})\right]$ is the measurement noise covariance matrix.

Step 4: compute the *a posteriori* state estimate:

$$\mathbf{x}_1^+(k) = \mathbf{x}_1^-(k) + \mathbf{K}(\mathrm{k})[\mathbf{z}_1(k) - \mathbf{C}_1(\mathrm{k})\mathbf{x}_1(\mathrm{k})] \tag{A.14}$$

Step 5: compute the *a posteriori* error covariance matrix:

$$\mathbf{P}^+(\mathrm{k}) = [\mathbf{I}_3 - \mathbf{K}(\mathrm{k})\mathbf{C}_1(\mathrm{k})]\mathbf{P}^{-1}(\mathrm{k}) \tag{A.15}$$

Then, the state estimate from (A.14) is $\mathbf{x}_1^+(\mathrm{k}) = [\mathbf{X}_{1,\mathrm{x}} \quad \mathbf{X}_{1,\mathrm{y}} \quad \mathbf{X}_{1,z}]^{\mathbf{T}}$. The roll and pitch angle can be found with the following equations:

$$\gamma(k) = \tan^{-1}\frac{X_{1,y}}{X_{1,z}} \tag{A.16}$$

$$\beta(\mathrm{k}) = \tan^{-1}\frac{-\mathrm{X}_{1,\mathrm{x}}}{\mathrm{X}_{1,y}/\mathrm{S}\gamma} \tag{A.17}$$

Yaw Kalman Filter

Using the roll and pitch angle obtained from the Tilt Kalman filter, the Yaw Kalman filter uses the following system model equations:

$$\mathbf{x}_2(\mathrm{k}) = \mathbf{A}_2(\mathrm{k}-1)\mathbf{x}_2(\mathrm{k}-1) + \mathbf{w}_2(\mathrm{k}-1) \tag{A.18}$$

$$\mathbf{z}_2(\mathrm{k}) = \mathbf{C}_2(\mathrm{k})\mathbf{x}_2(\mathrm{k}) + \mathbf{v_2}(\mathrm{k}) \tag{A.19}$$

where $\mathbf{x}_2 = [s\alpha c\beta \quad s\alpha s\beta s\gamma + c\alpha c\gamma \quad s\alpha s\beta c\gamma - c\alpha s\gamma]^{\mathrm{T}}$ is the state vector. $\mathbf{A}_2$, $\mathbf{w}_2$, $\mathbf{C_2}$ and $\mathbf{v}_2$ can be obtained with the following equations:

$$\mathbf{A}_2(\mathrm{k}-1) = \mathbf{I}_3 - \Delta\mathrm{t}\,\tilde{\mathbf{y}}_{\mathrm{G}}(\mathrm{k}-1) \tag{A.20}$$

$$\mathbf{w}_2(\mathrm{k}-1) = \Delta\mathrm{t}\left(-\tilde{\mathbf{x}}_2(\mathrm{k})\right)\mathbf{n}_{\mathrm{G}} \tag{A.21}$$

$$\mathbf{C_2}(\mathrm{k}) = \mathbf{I}_3 \tag{A.22}$$

$$\mathbf{v}_2(\mathrm{k}) = \mathbf{n}_M \tag{A.23}$$

where $\mathbf{n}_M$ is the magnetometer noise and is assumed to be a white noise.

In order to estimate the measurement vector, $\mathbf{z}_2$, magnetometer measurement, $\mathbf{y}_{\mathrm{M}}$, is first rotated to the navigation frame:

$$^{\mathrm{tilt}}\mathbf{y}_{\mathrm{M}} = {}^{\mathrm{N}}_{\mathrm{S}}\mathbf{R}_{\gamma,\beta}\mathbf{y}_{\mathrm{M}} \tag{A.24}$$

where ${}^{\mathrm{N}}_{\mathrm{S}}\mathbf{R}_{\gamma,\beta}\mathbf{y}_{\mathrm{M}} = \begin{bmatrix} c\beta & 0 & s\beta \\ 0 & 1 & 0 \\ -s\beta & 0 & c\beta \end{bmatrix}\begin{bmatrix} 1 & 0 & 0 \\ 0 & c\gamma & -s\gamma \\ 0 & s\gamma & c\gamma \end{bmatrix}$.

Once these matrices are calculated, the Yaw Kalman filter is calculated with the following steps:

Step 1: compute the *a priori* state estimates:

$$\mathbf{x}_2^-(k) = \mathbf{A}_2(\mathrm{k}-1)\mathbf{x}_2^+(k-1) \tag{A.25}$$

Step 2: compute the *a priori* error covariance matrix:

$$\mathbf{P}^-(\mathrm{k}) = \mathbf{A}_2(\mathrm{k}-1)\mathbf{P}^+(\mathrm{k}-1)\mathbf{A}_2^{\mathrm{T}}(\mathrm{k}-1) + \mathbf{Q}_2(\mathrm{k}-1) \tag{A.26}$$

where $\mathbf{Q}_2(\mathrm{k}-1) = \mathrm{E}\left[\mathbf{w}_2(\mathrm{k}-1)\mathbf{w}_2^{\mathrm{T}}(\mathrm{k}-1)\right]$ is the process noise covariance matrix.

Step 3: compute the Kalman gain:

$$\mathbf{K}(\mathrm{k}) = \mathbf{P}^-(\mathrm{k})\mathbf{C}_2^{\mathrm{T}}(\mathrm{k})\left[\mathbf{C}_2(\mathrm{k})\mathbf{P}^-(\mathrm{k})\mathbf{C}_2^{\mathrm{T}}(\mathrm{k}) + \mathbf{R}_2(\mathrm{k})\right]^{-1} \tag{A.27}$$

where $\mathbf{R}_2(\mathrm{k}) = \mathrm{E}\left[\mathbf{v}_2(\mathrm{k})\mathbf{v}_2^{\mathrm{T}}(\mathrm{k})\right]$ is the measurement noise covariance matrix. Here, conditions are set on $\mathbf{R}_2(\mathrm{k})$ to filter out potentially perturbed magnetic field data:

$$R_2(k) = \begin{cases} E\left[\mathbf{v}_2(k)\mathbf{v}_2^T(k)\right] & \left||\mathbf{y}_M - h|\right| < \varepsilon_M \\ \infty & Otherwise \end{cases} \quad (A.28)$$

Where h is the local earth's magnetic field and ε_M is the disturbance threshold.

Step 4: compute the *a posteriori* state estimate:

$$\mathbf{x}_2^+(k) = \mathbf{x}_2^-(k) + \mathbf{K}(k)[\mathbf{z}_2(k) - \mathbf{C}_2(k)\mathbf{x}_2(k)] \quad (A.29)$$

Step 5: compute the *a posteriori* error covariance matrix:

$$\mathbf{P}^+(k) = [\mathbf{I}_3 - \mathbf{K}(k)\mathbf{C}_2(k)]\mathbf{P}^{-1}(k) \quad (A.30)$$

With the a posteriori state estimate from (A.29), $\mathbf{x}_2^+(k) = [x_{2,x} \quad x_{2,y} \quad x_{2,z}]^T$, the best estimate for yaw angle, α can be calculated as:

$$\alpha(k) = \tan^- \left(\frac{-c\gamma x_{2,y} + s\gamma x_{2,z}}{x_{2,x}/c\beta}\right) \quad (A.31)$$

Appendix B.

Vertical Velocity/Position Kalman Filter

This is a summary of the Vertical Position/Velocity Kalman filter from [31]. The Vertical Position/Velocity Kalman filter requires the roll, γ and pitch, β input from Appendix A's Tilt Kalman filter.

The following system model equations are used in the Kalman filter to estimate vertical position and vertical velocity:

$$\mathbf{x}_2(\mathrm{k}) = \mathbf{A}_2(\mathrm{k}-1)\mathbf{x}_2(\mathrm{k}-1) + \mathbf{B}_2(\mathrm{k}-1)\mathrm{u}_2(\mathrm{k}-1) + \mathbf{w}_2(\mathrm{k}-1) \tag{B.1}$$

$$\mathbf{z}_2(\mathrm{k}) = \mathbf{C}_2(\mathrm{k})\mathbf{x}_2(\mathrm{k}) + \mathrm{v}_2(\mathrm{k}) \tag{B.2}$$

where $\mathbf{x}_2(\mathrm{k}) = [h(k) \quad v(k)]^T$ is the state vector. $\mathbf{A}_2$ and $\mathbf{B}_2$ are the state transition and input matrices, u_2 is the input vector, being the vertical component of gravity compensated acceleration in the navigation frame, $\mathbf{w}_2(\mathrm{k}-1)$ is the 2×1 process noise vector, $z_2(k)$ is the relative height ($\Delta \mathrm{h}_{baro}$), which is calculated from the barometric pressure data, $\mathbf{C}_2(\mathrm{k})$ and v_2 are the observation matrix and measurement noise. These variables are calculated as follows:

$$\mathbf{A}_2(\mathrm{k}-1) = \begin{bmatrix} 1 & \Delta t \\ 0 & 1 \end{bmatrix} \tag{B.3}$$

$$\mathbf{B}_2(\mathrm{k}-1) = \begin{bmatrix} \frac{1}{2}\Delta t^2 \\ \Delta t \end{bmatrix} \tag{B.4}$$

$$\mathrm{u}_2(\mathrm{k}-1) = ([0 \quad 0 \quad 1]) \cdot \left({}^{\mathrm{N}}_{\mathrm{S}}\mathbf{R}_{\gamma,\beta}\, {}^{\mathrm{S}}\mathbf{a}^{+}(\mathrm{k}-1) \right) \tag{B.5}$$

$${}^{\mathrm{N}}_{\mathrm{S}}\mathbf{R}_{\gamma,\beta} = \begin{bmatrix} c\beta & 0 & s\beta \\ 0 & 1 & 0 \\ -s\beta & 0 & c\beta \end{bmatrix} \begin{bmatrix} 1 & 0 & 0 \\ 0 & c\gamma & -s\gamma \\ 0 & s\gamma & c\gamma \end{bmatrix} \tag{B.6}$$

$$\mathbf{w}_2(\mathrm{k}-1) = \begin{bmatrix} \frac{1}{2}\Delta \mathrm{t}^2 \\ \Delta \mathrm{t} \end{bmatrix} \sigma_{\mathrm{A}} \tag{B.7}$$

$$z_2(k) \triangleq \Delta h_{baro} = 44330\left(1 - \left(\frac{p}{p_0}\right)^{0.19}\right) - h_{init} \tag{B.8}$$

$$C_2(k) = [1 \quad 0] \tag{B.9}$$

${}^{N}_{S}\mathbf{R}_{\gamma,\beta}$ is the rotation matrix that aligns the z-axis of sensor frame to the navigation frame. Δh_{baro} is the relative height with respect to the initial height (h_{init}) and P_0 is the standard pressure equal to 101,325 Pa.

Once these matrices are calculated, the Vertical Velocity/Position Kalman filter is calculated with the following steps:

Step 1: compute the *a priori* state estimates:

$$\mathbf{x}_2^-(k) = \mathbf{A}_2(\mathrm{k}-1)\mathbf{x}_2^+(k-1) \tag{B.10}$$

Step 2: compute the *a priori* error covariance matrix:

$$\mathbf{P}^-(\mathrm{k}) = \mathbf{A}_2(\mathrm{k}-1)\mathbf{P}^+(\mathrm{k}-1)\mathbf{A}_2^{\mathrm{T}}(\mathrm{k}-1) + \mathbf{Q}_2(\mathrm{k}-1) \tag{B.11}$$

where $\mathbf{Q}_2(\mathrm{k}-1) = \begin{bmatrix} \frac{1}{2}\Delta \mathrm{t}^2 \\ \Delta \mathrm{t} \end{bmatrix} \sigma_{\mathrm{A}}^2 \begin{bmatrix} \frac{1}{2}\Delta \mathrm{t}^2 \\ \Delta \mathrm{t} \end{bmatrix}^{\mathrm{T}}$ is the process noise covariance matrix.

Step 3: compute the Kalman gain:

$$\mathbf{K}(\mathrm{k}) = \mathbf{P}^-(\mathrm{k})\mathbf{C}_2^{\mathrm{T}}(\mathrm{k})\left[\mathbf{C}_2(\mathrm{k})\mathbf{P}^-(\mathrm{k})\mathbf{C}_2^{\mathrm{T}}(\mathrm{k}) + \mathrm{R}_2(\mathrm{k})\right]^{-1} \tag{B.12}$$

where $\mathrm{R}_2(\mathrm{k}) = \sigma_{\mathrm{baro}}^2$

Step 4: compute the *a posteriori* state estimate:

$$\mathbf{x}_2^+(k) = \mathbf{x}_2^-(k) + \mathbf{K}(\mathrm{k})[\mathbf{z}_2(k) - \mathbf{C}_2(\mathrm{k})\mathbf{x}_2(\mathrm{k})] \tag{B.13}$$

Step 5: compute the *a posteriori* error covariance matrix:

$$\mathbf{P}^+(\mathrm{k}) = [\mathbf{I}_2 - \mathbf{K}(\mathrm{k})\mathbf{C}_2(\mathrm{k})]\mathbf{P}^{-1}(\mathrm{k}) \tag{B.14}$$

The vertical position, $h(k)$ and velocity, $v(k)$ best estimate can be obtained from (B.13), where $\mathbf{x}_2^+(k) = [[h(k) \quad v(k)]^T]$.

Appendix C.

Ethics Approval

SFU OFFICE OF RESEARCH ETHICS

Street Address
Simon Fraser University
Discovery 2
Room 230, 8900 Nelson Way
Burnaby, BC Canada V5A 4W9

Mailing Address
8888 University Drive
Discovery 2
Burnaby, BC Canada
V5A 1S6

Director 778.782.6593
Associate Director 778.782.9631
Manager 778.782.3447
dore@sfu.ca
http://www.sfu.ca/ore.html

Annual Renewal Approval

Study Number: 2013s0790
Study Title: Advanced body motion and location tracking in active sports goggles

Annual Renewal Date: 2015 November 18
Expiry Date: 2016 November 18
Principal Investigator: Park, Edward
Supervisor: n/a
SFU Position: Faculty
Faculty/Department: Mechatronic Systems Engineering

SFU Collaborator: Zihajehzadeh, Shaghayegh
External Collaborator: Hoskinson, Reynald
Research Personnel: Lee, Matthew; Loh, Darrell; Yoon, Paul; Musngi, Magnus

Funding Source: NSERC
Grant Title: Advanced body motion and location tracking in active sports goggles

Documents Approved in this Application:

- Annual Renewal/Progress Report Form
- Annual renewal approval until November 18, 2016

The approval for this study expires on the **Expiry Date**. **Failure to submit an annual renewal form will lead to your study being suspended and potentially terminated.** If you intend to continue your protocol to collect data past the term of approval, you must submit an annual renewal/progress report at least 4 weeks before the expiry date at dore@sfu.ca.

Please notify the Office of Research Ethics at dore@sfu.ca once you have completed the data collection portion of your project so that we can close the file.

This Notification of Status is your official Annual Renewal Approval documentation for this project. Please keep this document for reference purposes.

Sincerely,

[redacted]

Holly Longstaff, PhD
Acting Associate Director, Office of Research Ethics